Sedimentary Geology 356 (2017) 26–42

Contents lists available at ScienceDirect

Sedimentary Geology

journal homepage: www.elsevier.com/locate/sedgeo

Detrital zircon fission-track thermochronology and magnetic fabric of the Amagá Formation (Colombia): Intracontinental deformation and exhumation events in the northwestern Andes

V.A. Piedrahita [a,*], M. Bernet [b], M. Chadima [c,d], G.M. Sierra [a], M.I. Marín-Cerón [a], G.E. Toro [a]

[a] Departamento de Ciencias de la Tierra, Universidad EAFIT, Medellín, Colombia
[b] Institut des Sciences de la Terre (ISTerre), Université Grenoble Alpes, Grenoble, France
[c] AGICO, Inc, Jecna 29a, CZ-62100 Brno, Czech Republic
[d] Institute of Geology of the CAS, v. v. i., Rozvojová 269, CZ-165 00 Prague 6 - Lysolaje, Czech Republic

ARTICLE INFO

Article history:
Received 27 February 2017
Received in revised form 19 May 2017
Accepted 21 May 2017
Available online 25 May 2017

Editor: Dr. B. Jones

Keywords:
Panama-Choco Block
Northern Andean Block
Amagá Formation
Zircon fission track
Anisotropy of magnetic susceptibility

ABSTRACT

New detrital zircon-fission track (ZFT) and magnetic fabric data are presented to constrain the time of deposition, provenance and deformation of the of Lower and Upper members of the Amagá Formation in the Amagá Basin. The Amagá Basin is located in the northern Andes, between the Western and Central Cordilleras of Colombia. The Amagá Formation was deposited in a transpressive geodynamic context and is allegedly synchronous with tectonic events such as the Andean orogeny and the Panama-Choco Block collision with the northwestern South American Plate. Detrital ZFT data confirm an Oligocene age for the Lower Member and a middle-Miocene age for the Upper Member of the Amagá Formation. In addition to constraining the depositional age, the ZFT data presented in this study also reflect Paleocene-Eocene, late to early Oligocene and late to middle Miocene cooling in sediment source areas mainly located in the Central and Western Cordilleras of Colombia. These ages can be associated with regional exhumation events in the central and northern Andes of South America. Collisional stages of the Panama-Choco Block against northwestern South America, subduction of the Farallon-Nazca Plate and strike-slip reactivation periods of the Cauca-Romeral fault system, caused NW-SE compression and NE-SW simple shear in the Amagá Basin. This deformational regime, identified by magnetic fabric data, induces syn- and post-depositional deformation over the Amagá Formation.

1. Introduction

The Cenozoic tectonic evolution of the northern Andes is mainly associated with the interaction between the South American, Caribbean and Farallon-Nazca plates, and the accretion of several tectonic blocks and terranes to the northwestern margin of the Northern Andean Block (NAB) (Cediel et al., 2003; Montes et al., 2005; Villagómez et al., 2011; Villagómez and Spikings, 2013). Subduction of the Farallon-Nazca and Caribbean plates beneath the South American Plate, the Eocene accretion of oceanic terranes (Kerr et al., 1997; Cediel et al., 2003; Echeverri et al., 2015) and the collision of the Panama-Choco Block (PCB) against the NAB (Coates et al., 2004; Farris et al., 2011; Montes et al., 2015; O'Dea et al., 2016), caused orogenesis and deformation in the northern Andes (Taboada et al., 2000; Cediel et al., 2003; Cortés and Angelier, 2005; Montes et al., 2005; Parra et al., 2009a; Parra et al., 2009b; Restrepo-Moreno et al., 2009; Farris et al., 2011; Villagómez et al., 2011; Villagómez and Spikings, 2013; Mora et al., 2015).

The events mentioned above occurred simultaneously with the formation of sedimentary basins along the Cauca depression, which is located in the inter-Andean valley between the Central and Western Cordilleras of Colombia (Fig. 1; Barrero et al., 2007; Sierra and Marín-Cerón, 2011). Those basins are called the Amagá – Cauca – Patía (ACP) Basins and their evolution is linked to the Cenozoic tectonic activity of the northern Andes (Acosta, 1978; Alfonso et al., 1994; Sierra and Marín-Cerón, 2011). The Amagá Basin is located in the northern part of the ACP Basins, close to the boundary between the NAB and the PCB (Fig. 1). This basin was formed in a continuously transpressive geodynamic context, linked to strike-slip reactivation periods of the Cauca-Romeral fault system, causing syn- and post-depositional deformation (Sierra and Marín-Cerón, 2011). The Amagá Formation, which constitutes part of the sedimentary infill of the Amagá Basin, was first determined to be of Paleogene to Neogene in age (Grosse, 1926; Van der Hammen, 1958). Given the location of the Amagá Basin between the Western and Central Cordilleras and the structural control of the Cauca-Romeral fault system on the basin evolution, the Amagá Formation functions as an archive of the Cenozoic tectonic events that occurred in this part of the northern Andes.

* Corresponding author.
E-mail address: vpiedra2@eafit.edu.co (V.A. Piedrahita).

http://dx.doi.org/10.1016/j.sedgeo.2017.05.003
0037-0738/

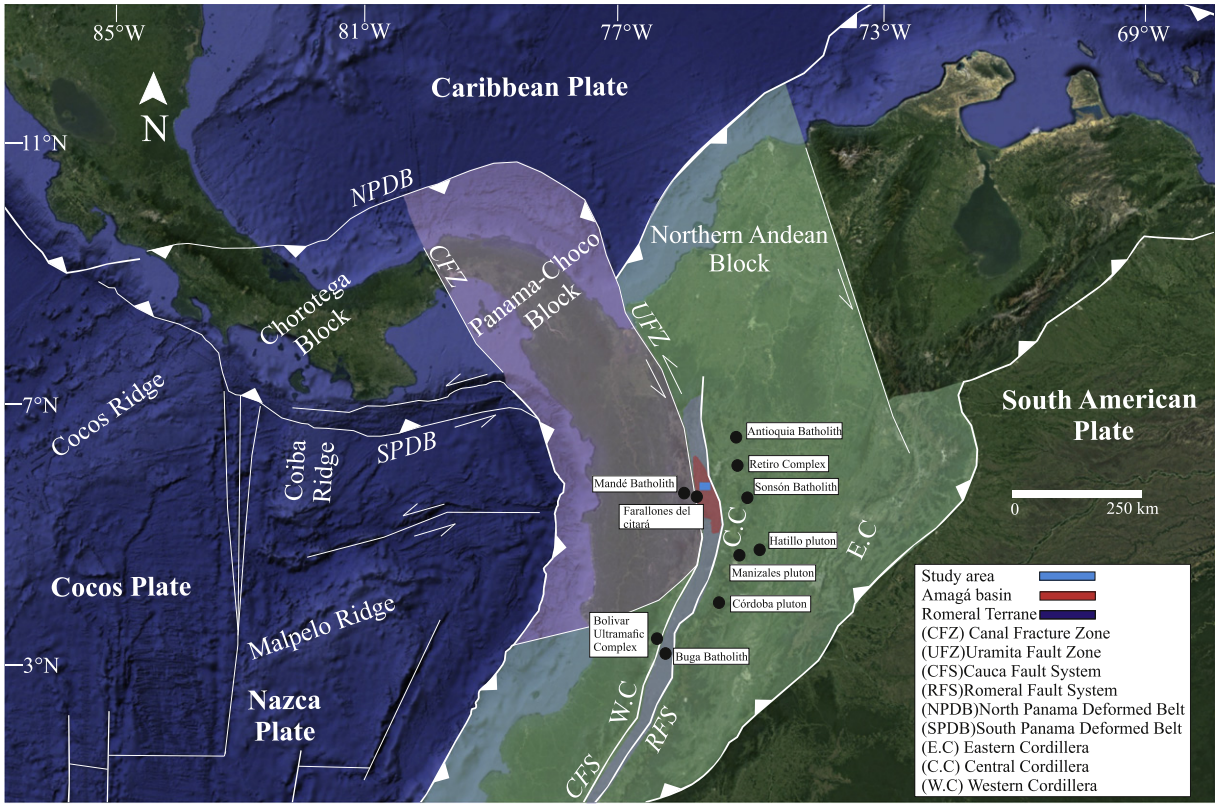

Fig. 1. Tectonic framework of the northwestern Andes including principal tectonic blocks, faults, the Romeral Terrane, the inter-Andean Amagá Basin and the possible source areas of the Amagá Formation (Cediel et al., 2003; Suter et al., 2008; Sierra and Marín- Cerón, 2011; Villagómez and Spikings, 2013). The Quebradagrande and Cajamarca complexes are located along the Romeral Terrane and Central Cordillera respectively.

The Cenozoic geological context of the northern Andes, and the location of the Amagá Basin, favored the deformation of the Amagá Formation in several deformational events (Sierra and Marín-Cerón, 2011). Those deformational events are evidenced by multiple Cenozoic reactivation periods of the Cauca-Romeral fault system (Sierra, 1994; Chicangana, 2005), as well as the presence of minor strike-slip, reverse and normal faults in the central part of the Amagá Basin (Grosse, 1926; Calle and González, 1980). Despite these observations, the deformational features of the Amagá Formation are not well described. The information related to the deformation of this unit is restricted to field observations and mapping which show that the deposition of the Amagá Formation was synorogenic and affected by deformation (Calle and González, 1980; Van der Hammen, 1958).

In this study, we present zircon fission-track (ZFT) thermochronological data of detrital zircon, from the same stratigraphic sections for which we have anisotropy of magnetic susceptibility (AMS) data. We pretend to study syn- and post-depositional deformation of the Amagá Formation. AMS and ZFT are very common methods in the study of sedimentary successions deposited in active tectonic settings (Gallagher et al., 1998; Aubourg et al., 2004; Bernet et al., 2006; Robion et al., 2007; Soto et al., 2009; Oliva-Urcia et al., 2013; García-Lasanta et al., 2014). Our anisotropy of magnetic susceptibility data is supported by thermomagnetic curves. The combination of techniques, which we presented in this work, allows us to gain new information on Cenozoic tectonic events in the northern Andes in terms of source area exhumation, timing of deposition in the basin and intracontinental deformation.

2. Geological setting

2.1. Regional geology

The Cenozoic tectonic framework of the northern Andes is related to the interaction between the Caribbean, Farallon-Nazca and South American plates (Fig. 1). The Nazca Plate is a result of the split of the Farallon Plate at ~23 Ma (Lonsdale, 2005). The oceanic Farallon-Nazca Plate was subducted beneath the western margin of the continental South American plate since the Mesozoic (e.g. Pindell and Kennan, 2009). During the Cretaceous, the Caribbean plate began an eastward migration to its current position north of the South American plate. All this generated re-activation of early Mesozoic or older faults, exhumation of rocks and important deformation in the northern Andes (Case et al., 1971; Pennington, 1981; Taboada et al., 2000; Montes et al., 2005; Parra et al., 2009a; Villagómez and Spikings, 2013).

The interactions between the South American, Caribbean and Farallon-Nazca plates favored the accretion of tectonic blocks and terranes to the northwestern margin of the Northern Andean Block (NAB). The NAB is a tectonic block located within the northwestern South American Plate. This tectonic block has been recognized as a distinct geological segment of the Andean Cordillera (Gansser, 1973; Cediel et al., 2003). Terranes of oceanic affinity and the NNW-SSE and NNE-SSW trending Cauca and Romeral strike-slip faults characterize the western part of the NAB (Fig. 1; Ego and Sébrier, 1995; Cediel et al., 2003). The Cauca fault limits the so-called Romeral Terrane, which consists of oceanic affinity rocks and mélange zones (Cediel et al., 2003). The Cauca fault is a suture zone with a right-lateral component, that separates the Romeral Terrane from the Dagüa-Piñon Terrane, which is another terrane of

oceanic affinity (Ego and Sébrier, 1995; Cediel et al., 2003). The Cauca fault activity is linked to the Romeral fault (Kammer, 1993; Ego and Sébrier, 1995), which constitutes the eastern boundary of the Romeral Terrane (Cediel et al., 2003). The Romeral fault separates oceanic crustal rocks from the continental rocks of the Central Cordillera of Colombian (Case et al., 1971; Chicangana, 2005). Ego and Sébrier (1995) confirmed a right lateral component for the Romeral fault. However, different reactivation periods of this fault during the Early Cretaceous, Late Cretaceous, Eocene, early Miocene, late Miocene, Pleistocene and Holocene, with alternating left-lateral and right-lateral motion, have been documented (Hutchings et al., 1981; Sierra, 1994; Chicangana, 2005; Cortés and Angelier, 2005; Sierra et al., 2012; Vinasco and Cordani, 2012). Of particular importance in this respect are the late Eocene accretion of an oceanic terrane (Kerr et al., 1997; Cediel et al., 2003; Echeverri et al., 2015) and late Oligocene to Mio-Pliocene (?) collision of the Panama-Choco Block (PCB) against the NAB (Coates et al., 2004; Farris et al., 2011; Montes et al., 2015; O'Dea et al., 2016).

The PCB consists of Meso-Cenozoic subduction-related and oceanic plateau igneous rocks (de Boer et al., 1991; Buchs et al., 2011; Wegner et al., 2011; Montes et al., 2012). Towards the northwest, this block is bounded by the Canal fracture zone (Lowrie et al., 1982; de Boer et al., 1991), which separates the PCB and the Chorotega Block (Fig. 1). In its southeastern area, the PCB borders the northwestern margin of South America along the Uramita fault zone (Fig. 1), which is characterized by its transpressional behavior and left-lateral component (Duque-Caro, 1990; Mann and Corrigan, 1990; Mann and Kolarsky, 1995). The PCB was accreted in E-SE direction to the northwestern margin of the NAB (Duque-Caro, 1990; Cortés and Angelier, 2005; Suter et al., 2008). The PCB collision and the continuous plate interactions in the northern Andes are evidenced by intracontinental deformation and several orogenic pulses with different exhumation rates (Taboada et al., 2000; Parra et al., 2009a; Restrepo-Moreno et al., 2009; Villagómez et al., 2011; Villagómez and Spikings, 2013; Mora et al., 2015).

In the northern Andes, different exhumation pulses have been documented in the three mountain ranges which constitute the Andean Cordillera in Colombia. The Eastern Cordillera of Colombia has a basement of Precambrian and Paleozoic metamorphic and igneous rocks, covered by Paleozoic to Mesozoic sedimentary successions (González et al., 1988). The Central Cordillera of Colombia consists of Precambrian high-grade metamorphic rocks, in contact with Paleozoic-Jurassic low-medium grade metamorphic rocks (Restrepo and Toussaint, 1988; Maya and González, 1995; Blanco-Quintero et al., 2014). All these metamorphic rocks were intruded by Permo-Triassic and Meso-Cenozoic igneous plutons (González et al., 1988; Cediel et al., 2003). The Western Cordillera of Colombia is characterized by Meso-Cenozoic allochthonous oceanic rocks, such as marine sediments and basaltic rocks. These rocks were intruded by Cenozoic igneous rocks and covered by volcanic successions (González et al., 1988). Several sedimentary basins, between the Colombian cordilleras, are located in the Magdalena River valley between the Eastern and Central Cordilleras and the Cauca depression between the Western and Central Cordilleras (Barrero et al., 2007). The ACP Basins are located in the so-called Cauca depression. The Amagá Basin is located in the northern region of the ACP Basins (Fig. 1) and is separated from the Cauca-Patía Basins by the Armenia alluvial Fan. The west and east limits of the Amagá Basin are given by the Cauca and Romeral faults, respectively (Sierra and Marín-Cerón, 2011). The sedimentary infill of the Amagá Basin, which was deposited in a transpressive regime, can be a record of the exhumation of the Western and Central Cordilleras of Colombia (Silva et al., 2008; Sierra and Marín-Cerón, 2011), as well as a marker of the accretion of the PCB against the NAB (Montes et al., 2015).

2.2. Local geology

The Amagá Basin is located in a mélange zone. Therefore, the basement of this basin consists of Triassic igneous and low-grade metamorphic rocks, which are in fault contact with Cretaceous rocks of oceanic affinity (Cediel et al., 2003; Sierra and Marín-Cerón, 2011). The Cretaceous oceanic affinity rocks, found in the Amagá Basin, belong to the Quebradagrande Complex. The Quebradagrande Complex consists of basalts, diabases and pyroclastic rocks, which are interlayered with cherts and siltstones (Calle and González, 1980). The Quebradagrande Complex was accreted to the western margin of the Northern Andean Block (NAB) during the Jurassic-Early Cretaceous (Cediel et al., 2003; Villagómez and Spikings, 2013). These rocks of oceanic affinity are in fault contact with low-grade metamorphic rocks such as phyllites and schists of the possibly Cretaceous Arquia Complex (González, 2001; Ruiz-Jiménez et al., 2012; Rodríguez and Arango, 2013). However, the age and lithostratigraphy of these rocks are not clearly determined, as Calle et al. (1980) mapped these rocks as Paleozoic-Jurassic low-grade metamorphic rocks of the Cajamarca Complex (Maya and González, 1995; Blanco-Quintero et al., 2014). The low-grade metamorphic rocks of the Amagá Basin basement are also in fault contact with Triassic igneous intrusive rocks belonging to the Pueblito Diorite and Romeral Gabbros (Fig. 2b) (Rodríguez-Jimenez, 2010).

The Amagá Formation, which is divided into a Lower and an Upper Member (Silva et al., 2008; Sierra and Marín-Cerón, 2011), was supposedly deposited from the Paleogene to the Neogene (Grosse, 1926; Van der Hammen, 1958; Ramírez et al., 2015). New palynological data in the northern Amagá Basin (Fig. 2a) suggest an Eocene-Miocene age of the Amagá Formation (Ramírez et al., 2015), whereas zircon U-Pb data indicate an Oligocene-early Miocene age for the Lower Member and a Middle Miocene age for the Upper Member of the Amagá Formation (Montes et al., 2015). The inconsistencies between the palynological and geochronological data, and the absence of geochronological information in other parts of the Amagá Basin show that the age of the Amagá Formation is not well known so far throughout the basin.

The Lower Member of the Amagá Formation (~294 m thick) was deposited in a continental fluvial environment of braided river systems with coarse-grained sandstones and conglomerates at the base bottom of the Albania and Excarbon sections (Fig. 3; Sierra et al., 2004; Silva et al., 2008). Subsequently, the deposition of the Lower Member was associated with meandering rivers, with fine-grained lithofacies associations of well-sorted sub-litharenites with high quartz content, massive gray siltstones, and coal layers (Silva et al., 2008; Sierra and Marín-Cerón, 2011). These rocks are observed in the Albania, Palomos and Excarbon sections, however, there are no clear correlations between these different stratigraphic sections (Fig. 3; Silva et al., 2008). Petrographic studies in sandstones of the Lower Member of the Amagá Formation show moderately-sorted and well-sorted medium-grained sandstones, which consist of polycrystalline and monocrystalline quartz, K-feldspar, plagioclase, metamorphic and plutonic rock fragments, and accessory minerals such as mica, amphibole, chlorite, pyroxene, apatite, zircon, garnet and rutile (Silva et al., 2008). These petrographic studies suggest that the source areas of the Lower Member of the Amagá Formation were in the Central and Western Cordilleras of Colombia, as well as, basement rock outcrops in the Amagá Basin (Grosse, 1926; Sierra et al., 2004; Silva et al., 2008; Sierra and Marín-Cerón, 2011).

The Upper Member of the Amagá Formation (~228 m thick) is characterized by exhibiting meandering river lithofacies at the bottom of the Venecia section, with interlayered mudstones and sandstones (Fig. 3). However, the depositional environment of the Upper Member changed to braided river environments with massive sandstones at the top of the Venecia section and the Cinco and Crisol sections (Silva et al., 2008). The Cinco section deposits are stratigraphically above the Venecia section and is overlain by the Crisol section deposits (Fig. 3; Sierra et al., 2004). The Upper Member of the Amagá Formation is characterized by lithic wackes, feldspathic litharenites and siltstones of reddish and greenish colors (Sierra and Marín-Cerón, 2011). The source areas of the Upper Member are mainly placed in the Central and Western Cordilleras of Colombia (Sierra et al., 2004; Silva et al., 2008; Sierra

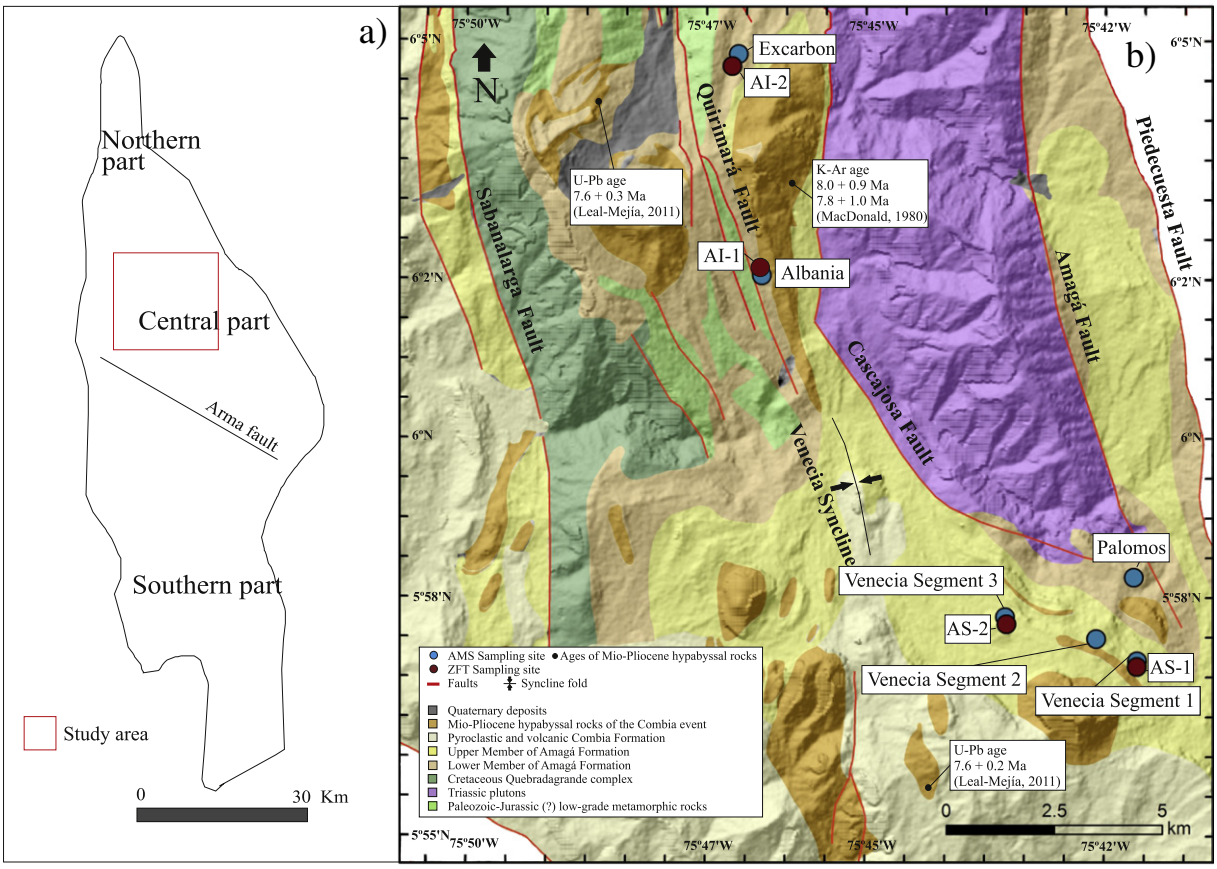

Fig. 2. (a) Schematic map of the Amagá Basin. (b) Geological map of the study area (Grosse, 1926; Calle et al., 1980) including sampling sites used in this study and ages of Mio-Pliocene hypabyssal rocks (MacDonald, 1980; Leal-Mejía, 2011).

and Marín-Cerón, 2011). However, Lara et al. (2015) and Montes et al. (2015) postulated that the rocks of the Upper Member may also have contributions of sediments from the PCB. Sandstones of the Upper Member consist of polycrystalline and monocrystalline quartz, K-feldspar, plagioclase, and metamorphic and plutonic rock fragments. The main compositional difference, between the sandstones of the Lower Member and the sandstones of the Upper Member of the Amagá Formation is the presence of sedimentary and volcaniclastic rock fragments in sandstones of the Upper Member of the Amagá Formation. Accessory minerals as magnetite, illmenite, apatite, zircon, garnet, pyroxene and amphibole were also described (Silva et al., 2008).

The Amagá Formation is overlain by the Mio-Pliocene Combia Formation. This unit consists of pyroclastic and volcanic rocks related to the volcanic Combia event (Grosse, 1926; Calle and González, 1980; Toro et al., 1999). The Combia event also has in its record hypabyssal rocks, which intrude the sedimentary rocks of the Amagá Basin (Fig. 2b) (MacDonald, 1980; Restrepo et al., 1981; Leal-Mejía, 2011).

The structural geology of the Amagá Basin is controlled by the Cauca-Romeral fault system. The most important fault in the Amagá Basin is the Sabanalarga strike-slip fault, which is located in the western sector of the study area and is identified by its Quaternary activity (Calle and González, 1980). In the central part of the study area, there are observed the Cascajosa normal fault and the Quirimará reverse fault (Fig. 2b; Grosse, 1926; Murillo, 1998). Finally, the eastern sector of the central Amagá Basin is characterized by the Amagá and Piedecuesta reverse faults (Grosse, 1926; Calle and González, 1980; Mejía et al., 1988). The structural style of the previously mentioned faults suggests several deformation events in the Amagá Basin (Grosse, 1926; Calle and González, 1980; Sierra and Marín-Cerón, 2011; Piedrahita et al., in press).

Local ductile deformation in the Amagá Basin is evidenced by folds such as the Venecia syncline, which is the only mapped fold in the study area and has a fold axis parallel to the NNW trend of the faults (Fig. 2b). There are also minor folds in the study area, but they have not been mapped due to their small extension therefore their characteristics are unknown (Calle and González, 1980). The deformational activity in the study area is also demonstrated by rotation of Mio-Pliocene intrusive rocks of the Combia event (MacDonald, 1980; MacDonald et al., 1996; Piedrahita et al., in press). Paleomagnetic and magnetic fabric studies of these hypabyssal rocks show that the igneous rocks intruded some layers of the Amagá Formation which had already been deformed, whilst other areas of the Amagá Formation were deformed post-intrusion (Piedrahita et al., in press).

3. Methods

3.1. Zircon fission track (ZFT)

Zircon fission-track (ZFT) dating is a well-established low-temperature thermochronology method, and fission-track analysis of detrital zircon has become a standard technique for studying sediment provenance, thermal history of rocks, long-term continental denudation and other geological processes (e.g. Hurford and Carter, 1991; Bernet and Garver, 2005). Fission tracks are produced by spontaneous fission of ^{238}U, ^{235}U and ^{232}Th isotopes (Price and Walker, 1963; Fleischer et al., 1975). However, the contribution from ^{235}U and ^{232}Th is negligible and only the accumulation of fission-tracks from ^{238}U is relevant (Wagner and Van den Haute, 1992). Particularly in sediment provenance and stratigraphic studies, the apparent ZFT cooling ages are interpreted in terms of cooling below the closure temperature of the

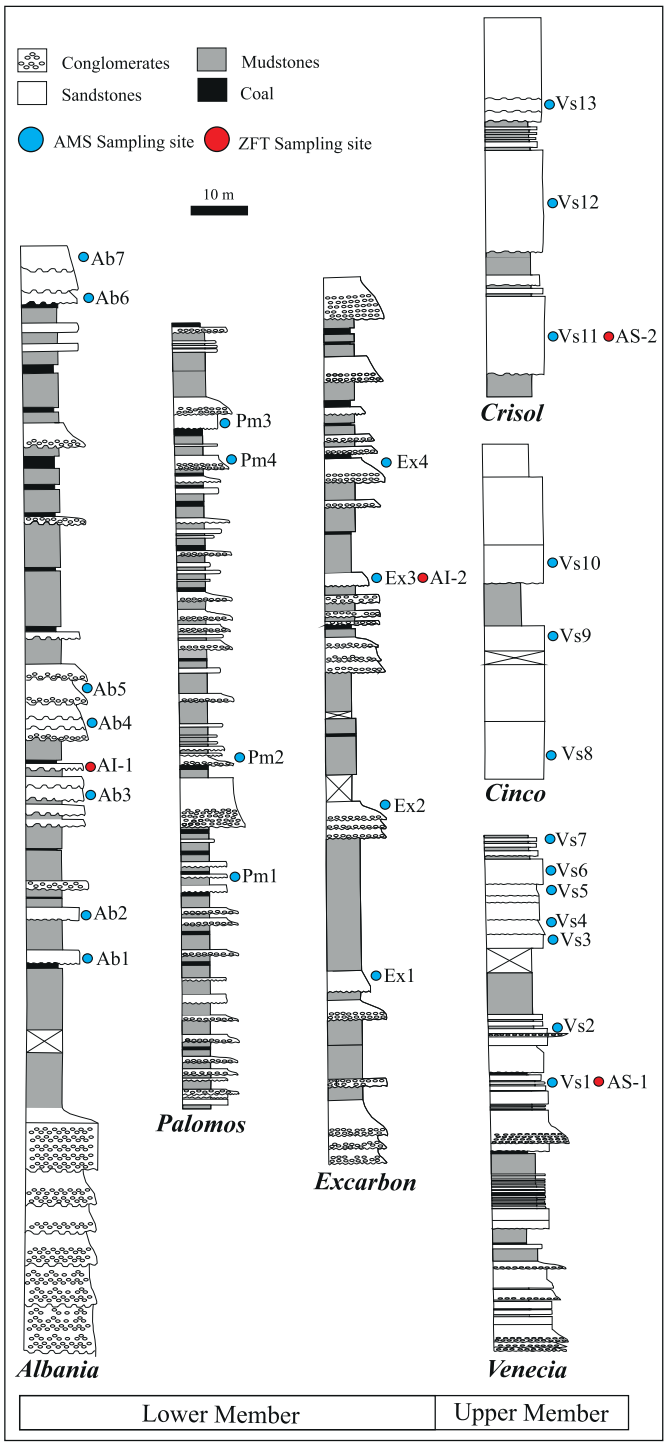

Fig. 3. Stratigraphic successions of the Amagá Formation, including sampling sites used in this study. All stratigraphic sections were taken from Sierra et al. (2004) and Silva et al. (2008).

fission-track system (e.g. Bernet and Garver, 2005; Reiners and Brandon, 2006). The closure temperature depends on the cooling rate, and for zircons also on the amount of accumulated radiation damage (Reiners and Brandon, 2006). For natural zircons in orogenic settings with common cooling rates on the order of 15 °C/Myr, the ZFT closure temperature is about 240 ± 20 °C (Brandon et al., 1998; Bernet, 2009).

Because detrital zircons in sedimentary rocks were derived from a variety of source rocks, with different cooling histories, it is possible to detect multiple grain age components or peaks in detrital grain age distributions by peak fitting (Galbraith and Green, 1990). The determined peak ages can be interpreted in terms of provenance, reflecting the cooling history of specific source areas (e.g. Bernet et al., 2004, 2006, 2009). Furthermore, the youngest age peak of a sample can be used as a first order estimate of the depositional age of the sampled rocks in the absence of post-depositional thermal resetting (Bernet and Garver, 2005). For additional information on fission-track dating, the interested reader can consult Wagner and Van den Haute (1992), Gallagher et al. (1998) or Tagami (2005).

For this study, about seven kilograms of sample were crushed and sieved. Zircons from fractions between 100 and 150 μm were separated from crushed rocks using density and magnetic separation techniques. Zircons were mounted in Teflon sheets, polished and etched in a solution of NaOH + KOH (11.2 g of KOH and 8 g of NaOH) at a constant temperature of 228 °C (Gleadow, 1981). Because we used the external detector method, grain mounts were covered with Kapton sheets as external detectors, and irradiated at the ORPHEE Saclay reactor (France), with a nominal fluence of 5×10^{15} neutrons/cm^2. Neutron fluency was monitored using CN1 dosimeter glasses. After irradiation, the Kapton sheets were etched in NaClO and 13 M HCl (100 ml of HClO by 4 g of NaCl) for 8 min in a boiling solution to reveal induced tracks.

We present ZFT data for two samples of the Lower Member and two samples of the Upper Member of the Amagá Formation (Fig. 2b, 3). Although it is recommended that over 100 grains should be dated per sample in detrital studies (Vermeesch, 2004), only between 42 and 69 grains were analyzed for our samples because of problems with metamict grains, U-zonation and other crystalline defects.

Fission-track ages were calculated using the *Z*-factor calibration method (Hurford and Green, 1983) and the *BinomFit* software (Brandon, 2002) to obtain grain-age distributions and major grain-age components or peaks. Even with the low number of analyzed grains per sample, reliable peak ages can be obtained when the peaks are well separated and contain >5% of the total number of analyzed grains (Vermeesch, 2014 personnel communication). All grains were dated wet at 1000× magnification using a biological Leica microscope at the *Laboratorio de investigación en Termocronología* (*Universidad Eafit*, *Colombia*).

3.2. Magnetic mineralogy

In order to characterize the carriers of magnetic fabric, magnetic susceptibility of six representative specimens (one of each stratigraphic section) was measured as a function of temperature using a KLY5-A Kappabridge coupled with CS-4 and CS-L temperature control units. Approximately 0.5 g of homogenized powdered specimen was investigated in a quartz glass test-tube with temperature being recorded by a platinum wire thermometer directly within the specimen powder.

First, in the low-temperature experiment, the specimens were spontaneously heated from the temperature close to liquid nitrogen (ca. −196 °C) up to the room temperature. Subsequently, in the high-temperature experiment, the same specimens were heated from room temperature up to 700 °C and cooled back to room temperature with a heating/cooling rate of ca. 14 °C/min. The high-temperature experiments were performed in a protective argon atmosphere to minimize any undesired mineral changes due to oxidation in elevated temperatures. During both experiments, magnetic susceptibility was measured approximately each 20 s.

The acquired curves of temperature variations of magnetic susceptibility were processed, visualized and analyzed using the *Cureval 8.0.2* software (www.agico.com). The curves were corrected for the respective empty cryostat/furnace and bulk susceptibility (i.e., volume-normalized), k_{bulk}, was calculated using the actual specimen mass and average density of sedimentary rocks ($\rho = 2.7$ g·cm^{-3}). For curves where hyperbolic decrease of magnetic susceptibility according to the Curie-Weiss Law is visually evident, the susceptibility resolution into

ferromagnetic and paramagnetic components based on the hyperbola fitting technique was employed (Hrouda, 1994; Hrouda et al., 1997).

3.3. Anisotropy of magnetic susceptibility (AMS)

Anisotropy of magnetic susceptibility (AMS) is a very sensitive method to visualize the preferred orientation of magnetic minerals in a rock. In sedimentary rocks, this technique may reflect different geological processes linked to the rock formation and/or its subsequent deformation (Graham, 1966; Hrouda, 1982; Borradaile, 1988; Averbuch et al., 1992; Tarling and Hrouda, 1993; Borradaile and Jackson, 2010). AMS is described as a second order symmetric tensor whose geometric representation is given by an ellipsoid with three axes ($K_1 \geq K_2 \geq K_3$). The orientation of the maximum principal axis defines a magnetic lineation and the perpendicular plane to the minimum principal axis (and containing the maximum and intermediate axes) defines a magnetic foliation; both elements defining a so-called magnetic fabric (Balsley and Buddington, 1960; Stacey et al., 1960; Tarling and Hrouda, 1993).

The magnitude and shape of the AMS ellipsoid can be described by a set of quantitative parameters. Those quantitative parameters are the shape parameter, T, the corrected anisotropy degree, P_j, and the mean magnetic susceptibility, K_m. The T parameter defines the shape of the anisotropy ellipsoid; this parameter ranges from -1 (linear magnetic fabrics) to $+1$ (planar magnetic fabrics). Values close to 0 indicate neutral or triaxial magnetic fabrics (Jelinek, 1981). The corrected anisotropy degree, P_j, shows the intensity of the preferred orientation of the minerals which control the magnetic fabric. Finally, the mean magnetic susceptibility, K_m, represents the bulk magnetic susceptibility (Nagata, 1961). K_m can provide information about the magnetic minerals presented in a rock, being an indicator of ferromagnetic or paramagnetic contributions to the magnetic fabrics (Rochette, 1987; Tarling and Hrouda, 1993; Borradaile, 2001). Traditionally, the identification of ferromagnetic and paramagnetic contribution is presented through the K_m-P_j plot (Rochette, 1987; Borradaile, 1988; Rochette et al., 1992; Borradaile, 2001). K_m values $>1000 \times 10^{-6}$ SI correspond to ferromagnetic minerals and K_m values $<1000 \times 10^{-6}$ SI characterize paramagnetic contributions (Rochette, 1987; Rochette et al., 1992; Tarling and Hrouda, 1993; Borradaile, 2001). Some authors describe paramagnetic-ferromagnetic mixed contributions to the magnetic fabrics with K_m values between ~500 and 1000×10^{-6} SI (Archanjo et al., 1999; Nagaraju et al., 2008). Despite the fact that low K_m values are related to paramagnetic minerals and high K_m values are linked to ferromagnetic minerals, this assumption should be always assessed through more accurate methods (i.e magnetic hysteresis measurements, thermomagnetic curves). Hirt et al. (2004) present cases which exhibit predominance of ferromagnetic carriers to magnetic fabrics with relatively low K_m values, whilst Raposo and Berquó (2008) show data for rocks with ferromagnetic components which are weakly orientated and do not correspond to the AMS carriers.

In addition to the conventionally used AMS parameters, we utilize two parameters which relate the magnetic fabric to the attitude of the strata of the sedimentary rocks. These parameters are l and f. The l parameter is defined as the angle between the bedding strike and the magnetic lineation, whilst the f parameter corresponds to the angle between the bedding and magnetic foliation (Tarling and Hrouda, 1993; Chadima et al., 2006).

Magnetic fabrics of sedimentary rocks are divided into sedimentary, intermediate or tectonic fabrics. According to the influence of deformation over the magnetic fabrics, six fabric types can be classified: I, II, III, IV, V, VI (Parés et al., 1999; Aubourg et al., 2004; Robion et al., 2007).

Sedimentary magnetic fabrics (Type I) are linked to undeformed rocks and are characterized by magnetic foliations parallel to the bedding ($f < \sim 25°$) and highly scattered magnetic lineations (Parés et al., 1999; Robion et al., 2007; Callot et al., 2010). Sedimentary fabrics are usually oblate and their anisotropy degree is low (Hamilton and Rees, 1970; Parés et al., 1999). Intermediate magnetic fabrics (type II and type III) are identified by early deformation stages, changes from oblate ellipsoids to prolate, triaxial (type III) or more pronounced oblate fabrics (type II) are produced. The magnetic lineation tends to be aligned perpendicular to the shortening direction, whilst the magnetic foliation is gradually deviated from the bedding. Low f values in fabrics type II progressively increase, showing fabrics type III (Robion et al., 2007; Soto et al., 2009; Callot et al., 2010). Tectonic magnetic fabrics (type IV, type V and type VI) are associated with deformational activity. These fabrics are characterized by high P_j values and changes in the AMS ellipsoid from prolate or neutral shapes in fabrics type IV to oblate shapes in fabrics type V and VI (Parés et al., 1999; Chadima et al., 2006; Robion et al., 2007). In tectonic magnetic fabrics, the angle f is high (>~65°; Callot et al., 2010) and the magnetic lineation is usually aligned following the direction of the cleavage/bedding intersection lines, gradually acquiring high inclinations (Robion et al., 2007).

For this magnetic fabric study, oriented cylindrical samples of 2.5 cm in diameter were collected using a gasoline-powered portable drill. On average 4 cylindrical cores per site were taken at 28 sites located in 6 stratigraphic successions of the Amagá Formation (Figs. 2b, 3). Only fine to medium grained sandstones were sampled. The attitude of the strata, at the sampling sites, was also recorded. In the laboratory, the samples were cut into specimens of 2.2 cm in height to yield a total of 166 standard cylindrical specimens.

The AMS was measured using a KLY-2 Kappabridge at the Colgate University, NY, USA. In order to obtain the AMS tensor, a sequence of 15 directional magnetic susceptibility measurements was carried out following the rotational design of Jelinek (1977). AMS data were processed using *Anisoft 4.2* software (Chadima and Jelinek, 2009) and presented using mean tensor statistics (Jelinek, 1981).

4. Results

4.1. Zircon fission track

ZFT results with central and peak ages are compiled in the Table 1, and shown in probability density and radial plots in Fig. 4. All errors are presented as 2σ errors. All samples have $P(x^2)$ values of zero, which are typical for over-dispersed detrital grain age distributions, showing a mixture of different grain-age components (Table 1; Galbraith, 1981). ZFT data from the Lower Member of the Amagá Formation are characterized by single-grain ages between 16.6 and 94.7 Ma (sample AI-1) and 20.0–90.6 Ma (sample AI-2).

Two populations for each sample are well defined (Fig. 4a, b). Sample AI-1 has age peaks at 57.5 ± 6.7 Ma (63.2% of dated grains) and 33.7 ± 5.5 Ma (36.8%) (Table 1, Fig. 4a, b). Sample AI-2 has an age peak at 49.1 ± 3.3 Ma (85.4%) and another age peak at 28.1 ± 5.8 Ma (14.6%) (Table 1, Fig. 4c, d).

ZFT data in the Upper Member of the Amagá Formation (Table 1) show three peaks for sample AS-1 at 56.5 ± 5.7 Ma (35.0%), 29.8 ± 3.8 Ma (26.1%) and 17.7 ± 1.6 Ma (38.9%). The single grain ages of these samples are between 11.3 and 78.5 Ma (Table 1, Fig. 4e, f). Sample AS-2 has four peaks at 50.4 ± 7.1 Ma (13.9%), 22.9 ± 2.8 Ma (30.9%), 15.6 ± 1.6 Ma (46.9%), and 10.6 ± 2.5 Ma (8.2%), with single grain ages between 9.6 and 86.2 Ma (Table 1, Fig. 4g, h).

4.2. Magnetic mineralogy

Based on the room temperature magnetic susceptibility, we can roughly distinguish two groups of specimens (Fig. 5): I) relatively low-susceptibility specimens Pm3 ($k_{bulk} = 7 \times 10^{-6}$ SI), Ex3 ($k_{bulk} = 124 \times 10^{-6}$ SI), Ab2 ($k_{bulk} = 347 \times 10^{-6}$ SI), and II) relatively high-susceptibility specimens Vs10 ($k_{bulk} = 2936 \times 10^{-6}$ SI), Vs4 ($k_{bulk} = 6319 \times 10^{-6}$ SI), Vs11 ($k_{bulk} = 11{,}117 \times 10^{-6}$ SI). The high-temperature treatment is highly irreversible for most specimens (except for Vs11) as the susceptibility on the cooling curves is about an order of magnitude higher compared to the respective heating curves

Table 1
Zircon fission-track data.

Sample	n	ρ_s (10^{+5} cm^{-2})	N_s	ρ_i (10^{+5} cm^{-2})	N_i	$P(\chi^2)$	Dispersion (%)	Age (Ma)*	±2 σ	U (ppm)	±1σ	Peak 1 (Fraction)	Peak 2 (Fraction)	Peak 3 (Fraction)	Peak 4 (Fraction)
AI-1	42	86.8	(4364)	21.0	(1055)	0.0	26.6	46.0	5.3	499	31	–	–	33.7 ± 5.5 36.8%	57.5 ± 6.7 63.2%
AI-2	54	55.6	(8472)	13.8	(2101)	0.0	20.7	45.0	3.8	328	14	–	–	28.1 ± 5.8 14.6%	49.1 ± 3.3 85.4%
AS-1	58	32.4	(6646)	12.3	(2528)	0.0	48.3	29.0	4.1	293	12	–	17.6 ± 1.6 38.9%	29.8 ± 3.8 26.1%	56.5 ± 5.7 35.0%
AS-2	69	35.2	(7114)	20.5	(4146)	0.0	39.7	19.6	2.2	488	15	10.6 ± 2.5 8.2%	15.5 ± 1.6 46.9%	22.9 ± 2.8 30.9%	50.4 ± 7.1 13.9%

Note: Fission-track age is given as central age (*) (Galbraith and Laslett, 1993). Ages were calculated using a *Z*-factor of 3.66E + 27.

(Fig. 5a, b). This irreversibility is most likely due to the growth of new magnetite, which starts to grow at the expense of paramagnetic minerals (most probably phyllosilicates) at elevated temperatures. This growth is manifested by a sharp susceptibility increase at ca. 400 °C, followed with a sharp decrease at ca. 570 °C when the Curie temperature of magnetite is achieved. Magnetite undoubtedly also grows at temperatures above 570 °C but its growth is not manifested by further susceptibility increase because at these temperatures magnetite behaves as a paramagnetic substance. New-grown magnetite is again evident on the cooling curves where we observe prominent peaks in susceptibility, with maxima in the range between 440 and 510 °C (Fig. 5a, b).

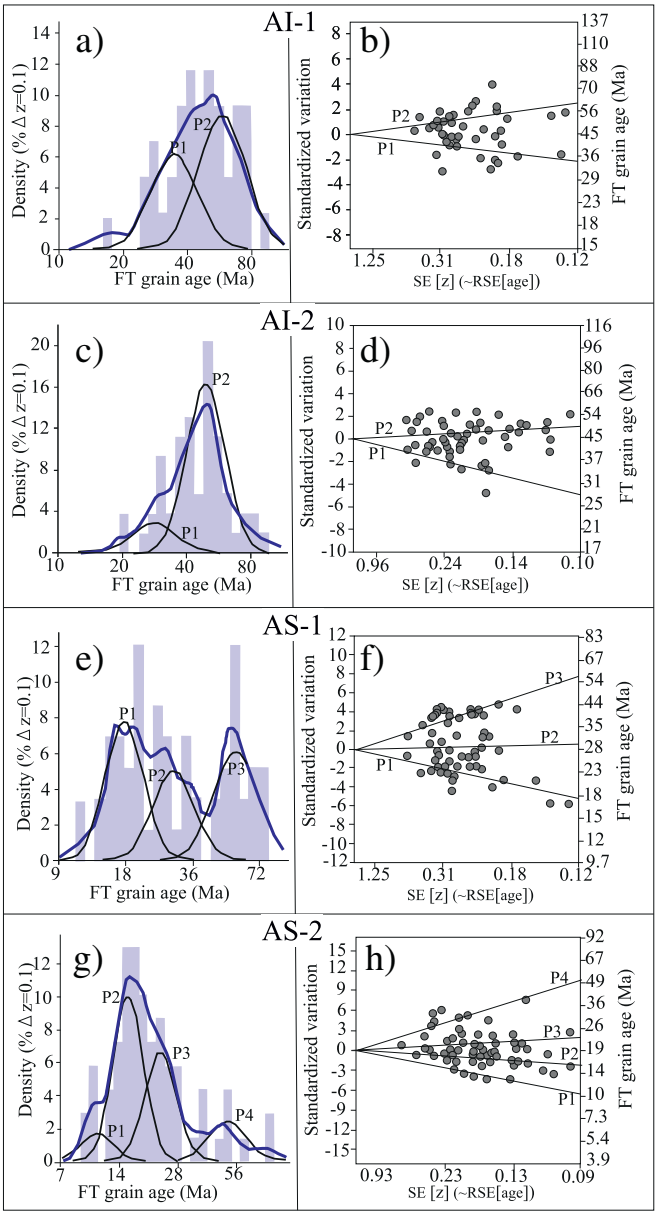

Fig. 4. Probability density with histograms and radial plots of zircon fission track data of all for all samples. The blue lines indicate the observed grain age distributions, main age peaks are shown as P1, P2, P3 or P4 (see Table 1). All graphs were made with *BinomFit* program of Brandon (2002). (a and b) Sample AI-1, (c and d) Sample AI-2, (e and f) Sample AS-1, (g and h) Sample AS-2.

The only quasi-reversible behavior is observed for the highest-susceptibility specimen Vs11 where the cooling curve follows more or less the trend of the heating curve implying that no mineral changes were induced during the high-temperature experiment. The magnetic mineralogy of this specimen is dominated by pure magnetite as it is clearly demonstrated by a pronounced Verwey transition (rapid change in susceptibility at ca. −160 °C) and the Curie temperature corresponding to pure magnetite (abrupt susceptibility decrease at ca. 570 °C, Fig. 5b). The presence of magnetite is also evident in all relatively high-susceptibility specimens (Vs4, Vs10, Vs11) where more or less pronounced "hump" on the low-temperature curves corresponding to the Verwey transitions is observed (Fig. 5b, c).

On the contrary, no Verwey transition is observed on the low-temperature curves of the relatively low-susceptibility specimens (Fig. 5c, Ab2, Ex3, Pm3). Magnetic susceptibility gradually decreases with increasing temperature following the course of a hyperbola, a behavior typical for paramagnetic minerals where susceptibility is inversely proportional to the absolute temperature. Following the susceptibility resolution technique of Hrouda (1994), and Hrouda et al. (1997), a hyperbola was fitted to each curve in the interval of −120 to 0 °C (Fig. 5c). For the low-susceptibility specimens, hyperbola fit is very good and the mathematical separation shows that more than a half of the magnetic susceptibility signal is carried by paramagnetic fraction (Fig. 5c: Ab2 ca. 85%, Ex3 ca. 60%, Pm3 ca. 65%). Interesting to note is that when we fit a hyperbola on the high-temperature curves in the interval of 30 to 250 °C (well below any susceptibility increase due to mineral changes), the course of that hyperbola meets the curve again at the highest temperatures, i.e. above ca. 570 °C (Fig. 5d). This provides an additional evidence that the observed magnetite has been only "artificially created" during the high temperature experiment and was not originally present in the unheated rock.

For the high-susceptibility specimens, hyperbola fit is very loose and the separation demonstrates that the magnetic susceptibility signal is almost exclusively carried by the ferromagnetic fraction and paramagnetic signal is negligible (Fig. 5c: Vs4 ca. 3%, Vs10 ca. 2%, Vs11 ca. 2%).

4.3. Magnetic fabric

4.3.1. Lower Member of the Amagá Formation

The Lower Member of the Amagá Formation is characterized by relatively low K_m values. The highest K_m value is 241 × 10^{-6} SI (Table 2). Two sampling sites, with negative K_m values and anomalous P_j values regard to the remaining sites, were identified. This is probably related to a high abundance of quartz in the samples of the two sites (Callot et al., 2010). Due to that fact, sites Ab1 and Ex4 were discarded from our interpretation.

All types of magnetic fabrics can be observed in our samples. A sedimentary magnetic fabric (8% of the sampling sites) was identified (Fig. 6b). Although this magnetic fabric is not clearly parallel to the

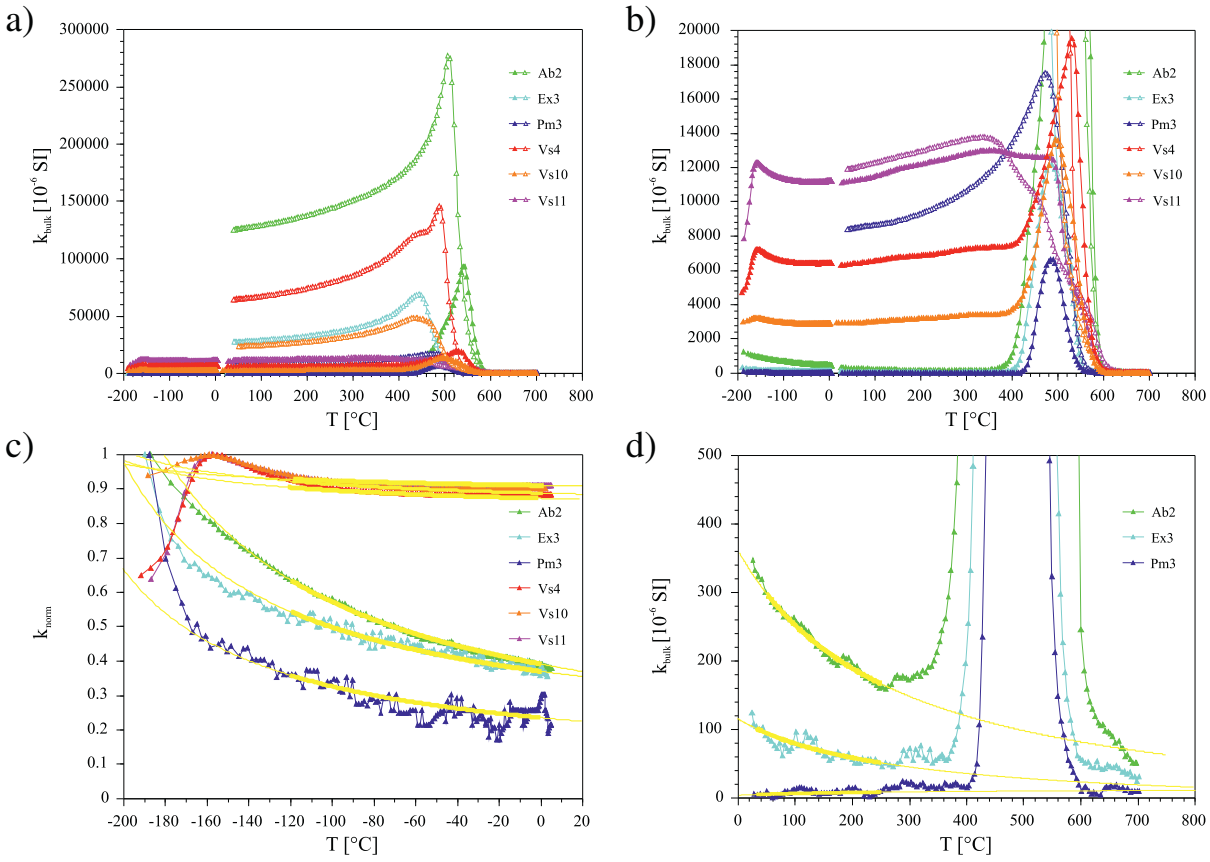

Fig. 5. (a) An overview of the low- and high-temperature curves (both for heating and cooling, closed and open symbols, respectively) of magnetic susceptibility of six representative specimens. (b) A detailed view showing the susceptibility interval from 0 to 20,000 × 10^{-6} SI. (c) A detailed view showing normalized low-temperature curves, fitted hyperbolas are shown as yellow lines. In bold is the interval where the fit was performed. (d) A detailed view of the high-temperature curves of three low-susceptibility specimens showing the susceptibility interval from 0 to 500 × 10^{-6} SI, fitted hyperbolas are as yellow lines, in bold is the interval where the fit was performed.

bedding plane at site Ex1. This site is characterized by a sub-vertical and well-clustered K_3 and scattered and sub-horizontal K_1.

Intermediate magnetic fabrics were identified in all of the Lower Member sections. Magnetic fabrics type II (15% of the sampling sites of the Lower Member) were only characterized in the Palomos section (Fig. 6b). Magnetic fabrics type II are identified by neutral to oblate AMS ellipsoids, whilst magnetic fabrics type III (31% of the sampling sites of the Lower Member) are mainly represented by prolate AMS ellipsoids.

All types of tectonic magnetic fabrics were detected in the Lower Member of the Amagá Formation. However, there are no tectonic magnetic fabrics in the Palomos section (Fig. 6b). Magnetic fabrics type IV (23% of the sampling sites of the Lower Member) are identified by neutral to prolate ellipsoids and sub-horizontal K_1 and K_3 axis. Magnetic fabrics type V (8% of the sampling sites) and type VI (15% of the sampling sites) were only identified in the Albania section. The magnetic fabric type V had a strongly oblate AMS ellipsoid with scattered K_1 and a vertical magnetic foliation. On the other hand, the magnetic fabrics type VI are characterized by neutral AMS ellipsoids with sub-vertical and well-clustered magnetic directions.

No relationships between K_m–P_j, K_m-T, P_j-l and P_j-f were observed for the successions Albania, Palomos and Excarbon (Fig. 6a, d, e, f). The high dispersion of T, l and f is linked to the presence of different magnetic fabric types. The only relationship between two AMS parameters was characterized for the Albania succession, which has a slightly negative relationship between P_j and T (Fig. 6c). This relationship may be associated with changes between intermediate and tectonic magnetic fabrics, and their respective variations of P_j and T. The Palomos and Excarbon sections do not have P_j-T relationships (Fig. 6c).

The magnetic lineations and magnetic foliations of the Albania and Palomos sections are highly scattered and do not represent good trends (Fig. 7). On the other hand, the magnetic directions of the Excarbon section are more closely clustered than the magnetic directions in the Lower Member of the Amagá Formation at the other sections. The magnetic lineations of this succession are mainly orientated in NE-SW and NW-SE directions, with a mean magnetic lineation towards the SW (Fig. 7). The magnetic foliations are sub-horizontal and have a slight preferential E-W strike.

4.3.2. Upper Member of the Amagá Formation

The Upper Member of the Amagá Formation has relatively high K_m values ($K_m > 10^{-6}$) which have a positive relationship with P_j and T (Fig. 6a, c, d). The progressive increase of K_m and the presence of magnetite (see section 4.2) show that increases in P_j and T are related to the distribution and magnetic interactions of magnetite grains (Grégoire et al., 1995), which control the magnetic fabric of the rocks of the Upper Member of the Amagá Formation.

Predominantly intermediate magnetic fabrics type II (67% of the sampling sites of the Upper Member) and type III (8% of the sampling sites of the Upper Member) were identified (Fig. 6b). Magnetic fabrics type II are observed in the Venecia and Cinco successions and are characterized by neutral to oblate AMS ellipsoids. Although the angle f for these magnetic fabrics are generally low ($f < \sim 25°$), the magnetic lineations are well clustered, exhibiting their intermediate type. Site Vs1 has a strongly prolate AMS ellipsoid and its K_1 and K_3 axis are interchanged regard to the remaining magnetic fabrics of the Venecia section. We suspect that the site Vs1 has an inverse magnetic fabric, even though the K_1

Table 2
AMS data of the Amagá Formation. n = Number of specimens, P_j = Corrected anisotropy degree, T = Shape parameter, K_m = Mean magnetic susceptibiliy, Strike/Dip = Attitude of the strata, K_1 = Declination and inclination of the maximum susceptibility axis, K_2 = Declination and inclination of the intermediate susceptibility axis, K_3 = Declination and inclination of the minimum susceptibility axis, l = Angle l, f = Angle f, Type = Magnetic fabric type.

	Succession	Site	n	P_j	St. Deviation	T	St. Deviation	K_m	St. Deviation	Strike/Dip	K_1 (°)	Conf.angle (°)	K_2 (°)	Conf.Angle (°)	K_3 (°)	Conf.Angle (°)	l (°)	St. Deviation	f (°)	St. Deviation	Type
Upper	Crisol	Vs13	6	1.01	0.011	−0.642	0.168	1.77E−04	9.39E−06	90/30	311.6/35.1	43.7/8.4	45.2/5.0	52.3/20.0	142.2/54.4	43.5/8.7	41.6	22.3	61.7	18.7	III
Member		Vs12	6	1.082	0.004	0.226	0.044	3.71E−03	3.41E−04	90/30	40.5/26.6	5.9/2.5	286.9/38.7	4.9/3.0	155.1/39.7	4.8/2.1	49.5	5.82	78.2	4.52	IV
of the Amagá		Vs11	6	1.17	0.025	0.693	0.065	1.12E−02	1.21E−03	90/30	49.5/4.3	6.4/2.7	316.1/38.3	6.4/2.7	144.9/51.3	3.8/1.9	40.5	4.14	65.2	2.79	V
Formation	Cinco	Vs10	6	1.13	0.006	0.854	0.039	2.22E−03	2.75E−04	90/30	270.6/3.7	12.5/2.9	4.0/42.2	12.5/3.2	176.5/47.6	3.3/3.1	0.6	10.6	72.4	3.29	V
		Vs9	6	1.081	0.03	0.747	0.174	6.15E−04	2.81E−04	216/20	83.9/16.0	26.4/3.0	349.6/14.5	26.4/5.5	219.5/68.1	5.8/2.6	47.9	17.1	30.2	3.39	II
		Vs8	6	1.059	0.01	0.301	0.167	2.24E−04	1.80E−06	216/20	249.1/11.9	5.8/2.3	339.2/0.5	8.3/3.3	71.6/78.0	7.3/3.3	33.1	5.48	16.1	4.04	II
	Venecia	Vs7	6	1.062	0.007	0.745	0.074	5.15E−03	1.54E−03	216/20	70.7/5.9	17.6/4.2	160.7/0.7	16.6/2.5	257.4/84.1	7.8/2.2	34.7	69.5	24.3	25.8	II
		Vs6	6	1.223	0.119	0.812	0.109	2.55E−02	1.18E−02	216/20	43.0/1.0	9.9/4.2	312.9/4.3	10.2/2.3	146.3/85.6	6.6/3.2	7.0	10.9	15.9	6.96	II
		Vs5	6	1.057	0.008	0.173	0.122	1.81E−03	5.46E−04	216/20	228.9/5.5	8.8/1.2	138.8/0.5	8.1/3.6	43.9/84.4	6.1/2.3	12.9	22.3	20.0	2.86	II
		Vs4	6	1.069	0.002	0.44	0.192	5.13E−03	5.53E−04	216/20	52.5/3.8	4.0/3.6	322.0/7.1	3.9/3.7	170.6/81.9	5.1/0.5	16.5	22.5	15.3	7.81	II
		Vs3	6	1.113	0.021	0.541	0.081	3.16E−03	9.63E−04	216/20	242.1/2.3	2.9/0.9	332.5/9.9	3.6/1.3	139.2/79.8	3.8/1.5	26.1	2.14	10.3	3.76	II
		Vs2	6	1.126	0.012	0.729	0.031	4.75E−03	8.26E−04	216/20	69.0/16.9	5.5/1.6	333.6/17.6	5.4/3.4	200.7/65.4	3.8/1.8	33.0	31.3	26.9	26.3	II
		Vs1*	7	1.105	0.017	−0.958	0.11	1.11E−04	2.66E−05	130/20	285.8/69.9	14.2/2.4	147.6/15.3	67.0/13.3	54.0/12.8	67.0/3.0	24.2	20.4	57.9	24.4	III
Lower	Excarbon	Ex4*	5	1.198	0.245	0.316	0.267	−3.98E−06	3.33E−06	78/35	336.7/5.2	22.6/9.3	234.9/65.9	32.3/11.9	69.0/23.4	28.3/11.8	78.7	38.2	65.9	24.7	IV
Member		Ex3	6	1.008	0.017	0.246	0.388	2.41E−04	5.05E−05	78/35	274.2/4.4	32.8/4.1	12.0/60.5	50.0/17.0	181.7/29.2	46.3/4.9	16.2	17.5	85.0	26.1	IV
of the Amagá		Ex2	6	1.029	0.009	−0.427	0.565	2.84E−05	7.44E−06	78/35	221.3/2.3	6.3/4.8	312.9/35.2	12.2/5.0	128.0/54.7	12.7/4.1	36.7	14.2	65.5	24.9	III
Formation		Ex1	5	1.041	0.035	0.765	0.439	1.71E−05	1.23E−05	78/35	76.2/0.5	63.2/7.7	166.3/3.0	63.0/15.9	337.1/87.0	18.1/16.6	1.8	21.4	32.1	14.6	I
	Palomos	Pm4	6	1.008	0.007	−0.339	0.381	1.03E−04	5.33E−05	128/15	347.6/19.9	15.9/6.5	91.9/34.2	66.1/9.3	233.0/48.9	66.1/13.8	39.6	46.0	55.7	39.0	III
		Pm3	6	1.002	0.002	−0.904	0.366	6.34E−05	1.29E−05	128/15	168.1/18.5	38.6/29.7	303.8/64.9	87.1/36.6	72.4/16.3	87.1/23.2	40.1	80.1	61.6	36.5	III
		Pm2	6	1.025	0.038	−0.026	0.549	5.60E−05	1.87E−05	285/20	265/37.3	43.5/36.8	9.7/18.4	43.5/30.3	120.4/46.9	37.4/29.4	20.0	26.6	41.6	21.0	II
		Pm1	5	1.009	0.03	0.125	0.22	4.74E−05	5.91E−06	285/20	138.6/32.9	59.9/26.6	231.9/5.2	65.2/18.9	329.9/56.6	54.7/23.2	33.6	25.5	49.3	18.5	II
	Albania	Ab7	6	1.031	0.006	−0.183	0.217	4.24E−05	5.88E−06	72/44	194.0/62.3	7.4/1.6	13.3/27.7	6.7/3.4	103.4/0.3	4.5/3.9	58.0	1.64	69	2.31	VI
		Ab6	6	1.006	0.003	0.177	0.417	2.28E−05	7.26E−06	72/38	275.6/18.1	51.8/23.2	28.5/50.0	50.4/26.4	172.8/34.3	34.8/26.4	23.6	47.5	86.8	71.1	IV
		Ab5	6	1.031	0.05	−0.367	0.486	2.93E−05	5.92E−06	72/38	67.8/19.1	27.6/3.9	161.8/11.5	44.8/10.0	281.2/67.5	46.1/12.5	4.2	26.2	32.5	16.4	III
		Ab4	6	1.028	0.009	0.04	0.31	4.58E−05	8.97E−06	72/44	314.7/22.4	3.7/1.8	52.5/18.4	5.1/1.8	178.3/60.4	4.8/1.4	62.7	23.3	72.8	20.7	IV
		Ab3	6	1.026	0.01	−0.154	0.249	8.44E−05	2.80E−05	72/44	205.0/68.5	13.6/5.7	13.9/21.1	16.6/12.6	105.3/3.8	17.1/3.3	47.0	9.43	70.6	6.60	VI
		Ab2	6	1.01	0.005	0.748	0.175	1.93E−04	6.26E−05	72/38	305.7/10.8	47.2/7.1	38.8/16.0	47.2/9.1	183.1/70.5	13.0/5.7	53.7	23.8	56.6	22.2	V
		Ab1*	6	1.360	0.545	−0.644	0.144	−2.17E−06	5.94E−07	72/44	225.1/4.5	31.3/2.9	117.5/75.4	31.4/2.8	316.2/13.6	6.4/2.6	26.9	13.2	39.0	7.12	III

Note: Our data are presented using mean tensor statistics (Jelinek, 1981). Principal susceptibility axes are shown in paleographic coordinate system.

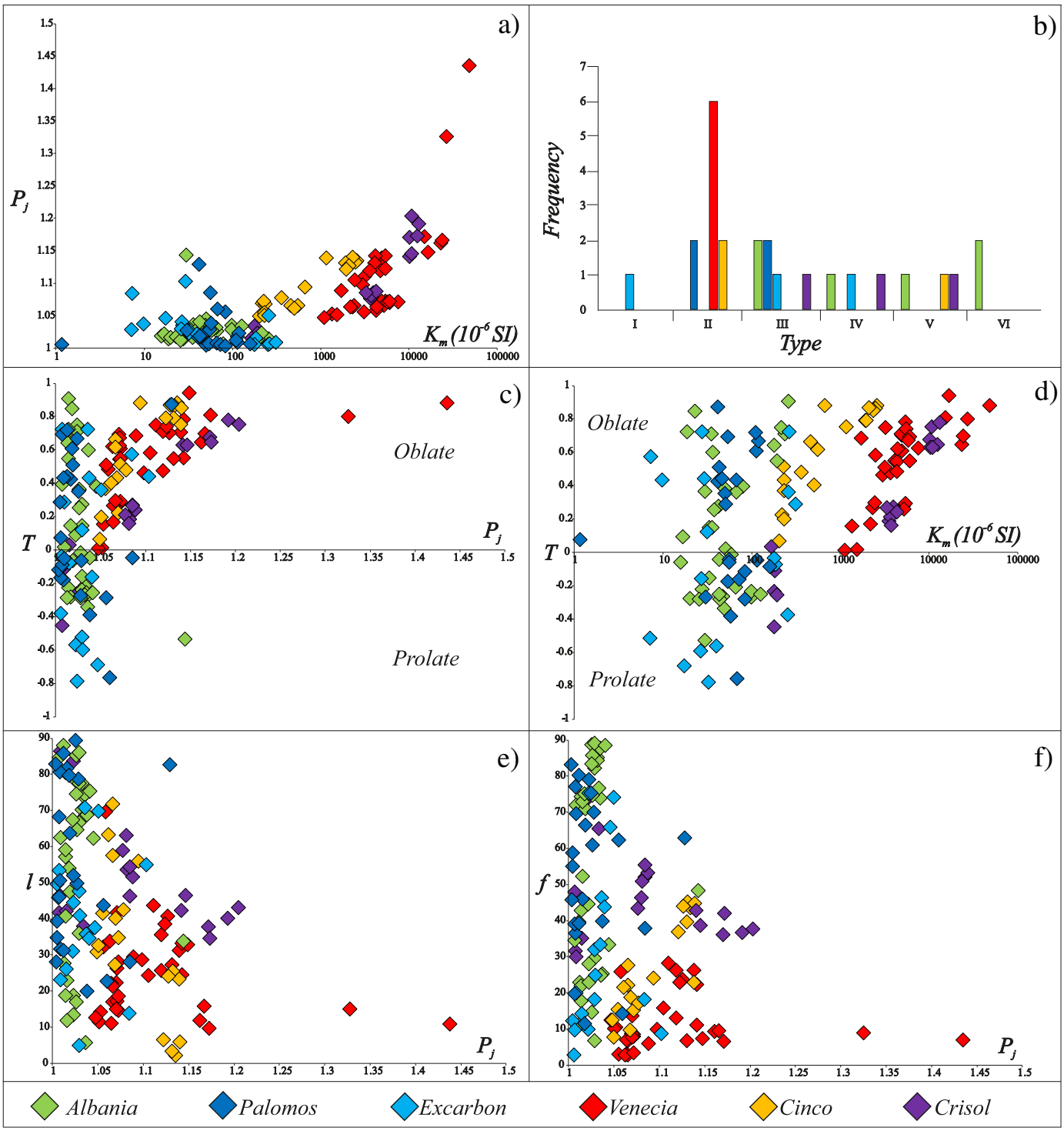

Fig. 6. (a) Correlation between K_m and P_j. (b) Frequency distribution of magnetic fabric types. (c) Correlation between P_j and T. (d) Correlation between K_m and T. (e) Correlation between P_j and l. (f) Correlation between P_j and f. The parameters P_j, T, l and f are shown using mean tensor statistics (Jelinek, 1981). The bulk susceptibility is described using the K_m parameter (Nagata, 1961).

is not clearly perpendicular to the bedding (Winkler et al., 1996). Due to that fact, we have discarded this site from our interpretation.

Tectonic magnetic fabrics type IV (8% of the sampling sites of the Upper Member) and V (17% of the sampling sites of the Upper Member) were identified in the Cinco and Crisol sections and are characterized by magnetic fabrics with high f angles (>65°) and neutral to oblate AMS ellipsoids.

No relationships in the P_j-l and P_j-f plots of the Venecia section were identified (Fig. 6e, f). However, there are negative relationships in the P_j-l plot for the successions Cinco and Crisol (Fig. 6e). These relationships are linked to the re-orientation of the magnetic lineations due to the transition from intermediate to tectonic magnetic fabrics (Chadima et al., 2006; Robion et al., 2007). The P_j-f plot shows a positive relationship for the Cinco succession (Fig. 6f), which may be associated

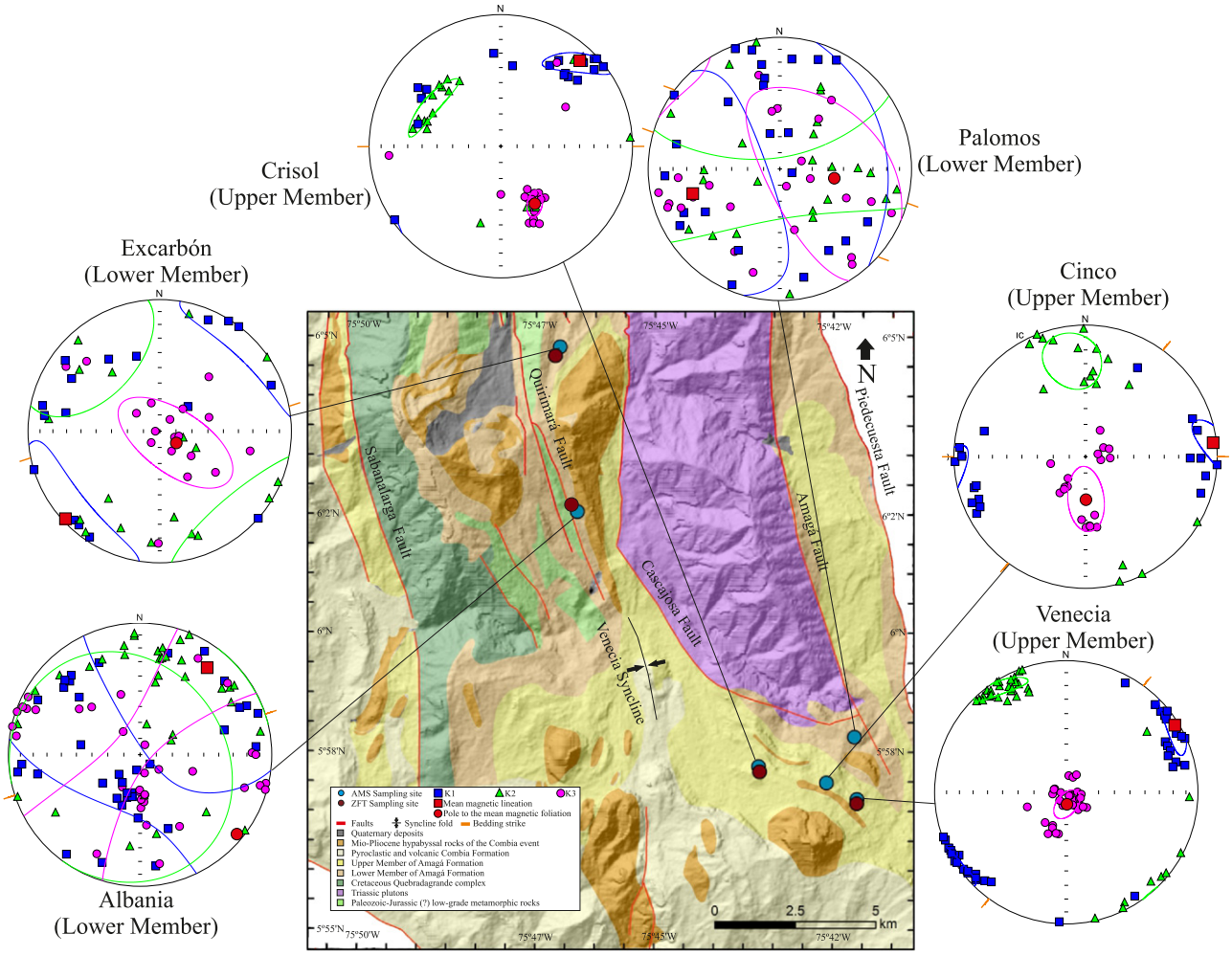

Fig. 7. Stereographic projections of the AMS data (all specimens). All data are projected in the lower-hemisphere, equal-area and paleo-geographic coordinate system (Table 2).

with the change from intermediate magnetic fabrics type II to tectonic magnetic fabrics type V. No relationship between P_j and f was observed for the Crisol section.

Well-defined clusters of the K_1 and K_3 axes characterize the Upper Member of the Amagá Formation (Fig. 7). The magnetic lineations, in the Upper Member, are identified by NE-SW to E-W trends and sub-horizontal plunges. On the other hand, the magnetic foliations have sub-horizontal to intermediate dips with preferential strikes in E-W and NE-SW directions.

5. Discussion

5.1. Depositional age and provenance of the Amagá Formation sediments

Vitrinite reflectance r data of in general %Ro = ~0.5 has been reported for the Amagá Basin, which indicates a maximum burial depth of ~2 km, for a common geothermal gradient between 25 °C/km and 30 °C/km (Pérez, 2013). There are local variations in vitrinite reflectance, values of up to %Ro = ~3, related to Mio-Pliocene hypabyssal intrusions of the Combia event (Arrubla, 2012; Pérez, 2013). However, the Amagá Formation at the sampling locations was not thermally affected by the Combia event and the zircon fission-track grain-age components presented in this study are interpreted here reflecting source area cooling and not post-depositional partial resetting.

The oldest age peaks in our ZFT data have late Paleocene to early Eocene apparent cooling ages. These peaks are observed in both the Lower Member (57.5 ± 6.7 and 49.1 ± 3.3) and Upper members of the Amagá Formation (56.5 ± 5.7 and 50.4 ± 7.1). Similar ZFT ages have been determined in rocks of the Central Cordillera of Colombia, such as the Precambrian Retiro Complex, with ZFT ages between 60.8 ± 1.7 and 46.7 ± 1.2 Ma (Montes, 2007), and the Cajamarca Complex, with ZFT ages ranging from 63.6 ± 9.4 to 47.0 ± 9.0 Ma (Villagómez and Spikings, 2013). Cretaceous-Paleocene igneous rocks, which intruded the Retiro and Cajamarca complexes, also have several Paleocene-Eocene ZFT ages, i.e. Antioquia and Sonsón batholiths (ZFT ages between 65.5 ± 6.0 and 47.9 ± 5.2 Ma), and the Córdoba, Hatillo and Manizales plutons (ZFT ages from 55.3 ± 5.4 to 43.9 ± 4.2) (Fig. 1; Villagómez and Spikings, 2013).

West of the Romeral fault, the Cauca depression and the Western Cordillera of Colombia also have units with Paleocene-Eocene ZFT ages. The Cretaceous Quebradagrande Complex has two Paleocene-Eocene ZFT ages of 64.5 ± 14.6 and 51.8 ± 7.4, the Bolivar Ultramafic Complex presents a Paleocene-Eocene ZFT age of 62.5 ± 5.2 and the Buga batholith has a ZFT age of 41.3 ± 4.2 (Fig. 1; Villagómez and Spikings, 2013). Therefore, zircons with Paleocene to Eocene fission-track cooling ages, found in the Amagá Formation, where most likely derived from source areas adjacent to the ACP Basins, in the Central and Western Cordilleras of Colombia. Because of the similarity in the ZFT ages in the Western and Central Cordillera, it is not possible to determine by the ZFT age alone from which side of the basin the zircons arrived. However, given the very low zircon fertility of many rocks of oceanic affinity the Western Cordillera, it is more likely that the majority of these zircons were derived from the more acid crystalline rocks of the Central Cordillera. This interpretation is consistent with previous

petrographic studies (Murillo, 1998; Hernández, 1999; Silva et al., 2008; Moreno-Quimbay, 2011; Henao-Betancur, 2012; Pérez, 2013). The Mandé Batholith, which is located within the Panama-Choco Block (PCB), has ZFT ages of 46.4 ± 5.8 and 41.6 ± 5.4 Ma (Villagómez and Spikings, 2013), however, there is no direct evidence that the PCB provided sediments to the Lower Member of the Amagá Formation (Lara et al., 2015; Montes et al., 2015).

Early Oligocene to early Miocene ZFT peak ages are observed in both members of the Amagá Formation. There are ZFT peak ages of 33.7 ± 5.5 and 28.1 ± 5.8 in the Lower Member of the Amagá Formation, whilst peak ages of 29.8 ± 3.8 and 22.9 ± 2.8 were identified in the Upper Member of this unit. These ZFT ages are similar to ZFT ages of 39.3 ± 12.0 and 38.7 ± 18.0 of the Cajamarca complex (Villagómez and Spikings, 2013). Although the Cajamarca complex is a likely source of zircons with Oligocene-early Miocene cooling ages, it is also possible that some of these were derived from sources in the Western and Central Cordilleras that have not yet been dated with the ZFT method.

The youngest age peak of the Lower Member of the Amagá Formation is 28.1 ± 5.8. Therefore, an Oligocene age is assigned for this succession as a first order estimate at the given sampling location. This depositional age is slightly older than the Oligocene-early Miocene depositional age assigned by Montes et al. (2015) to the Lower Member of the Amagá Formation in the northern Amagá Basin. This difference may be related to the exact stratigraphic position and the area where the samples were collected. At this stage, no direct correlation of the Lower Member is possible between the different parts of the basin.

The youngest age peaks of the Upper Member samples of the Amagá Formation are at 17.6 ± 1.6, 15.5 ± 1.6 and 10.6 ± 2.5, suggesting an early to middle Miocene age of deposition, possibly also younger. So far early to middle Miocene ZFT ages have been recorded in the Eastern Cordillera of Colombia (Parra et al., 2009a; Parra et al., 2009b; Amaya et al., 2017). However, unpublished ZFT ages between 9 and 17 Ma of Restrepo-Moreno et al. from the Farallones del Citara in the Western Cordillera of Colombia (Fig. 1) show that potential source areas exist in the vicinity of the Amagá Basin. Nonetheless, further research is needed to identify source areas.

The youngest age peak of sample AS-2 (10.6 ± 2.5 Ma) from the Upper Member of the Amagá Formation is slightly younger than the depositional age of 13.3 ± 0.4 Ma proposed by Montes et al. (2015) for the Upper Member of the Amagá Formation, in the northern Amagá Basin. The age of 10.6 ± 2.5 Ma overlaps the volcanic Combia event (12–6 Ma, Mesa-García, 2015), however, it does not correspond to a partial resetting age. The population of 10.6 ± 2.5 belongs to the Sample AS-2, which is located close to hypabyssal intrusive rocks with U-Pb ages of 7.6 ± 0.2 Ma and 7.6 ± 0.3 Ma (Leal-Mejía, 2011), and K-Ar ages of 8.0 + 0.9 Ma and 7.8 + 1.0 Ma (MacDonald, 1980) (Fig. 2b). Therefore, it is not possible that the age of 10.6 ± 2.5 corresponds to a thermal event.

It is possible that the 10.6 ± 2.5 Ma peak age is be related to the first eruptive episodes of the Combia event, but this needs to be confirmed through zircon fission-track and U-Pb single grain double-dating. At least the pyroclastic rocks of the Combia Formation have ZFT ages between ~12.0 and ~6 Ma (Mesa-García, 2015), and the presence of volcanic fragments from the Combia Formation in the sandstones of the Upper Member of the Amagá Formation support this possibility (Silva et al., 2008).

5.2. Rock magnetism, magnetic fabric and deformation of the Amagá Formation

The thermomagnetic curves of samples from the Lower Member of the Amagá Formation are characterized by relatively low room-temperature susceptibility values, absences of Verwey transitions and low-temperature curves showing a hyperbolic decrease of susceptibility with increasing temperature (Fig. 5). Those samples also possess relatively low K_m values (Fig. 6a). These features are common for paramagnetic minerals and may be related to phyllosilicates as muscovite and chlorite or paramagnetic silicates as hornblende and biotite. These minerals are found in the mineralogy of the Lower Member of the Amagá Formation (Murillo, 1998; Henao-Betancur, 2012). The samples of the Upper Member of the Amagá Formation are characterized by relatively high susceptibility values, pronounced Verwey transitions and evident Curie points related to magnetite (Fig. 5) with relatively high K_m values (Fig. 6a).

Petrographic studies carried out in the Amagá Formation (e.g Murillo, 1998; Hernández, 1999; Moreno-Quimbay, 2011; Henao-Betancur, 2012; Silva et al., 2008), our ZFT analyses and the magnetic mineralogy results show different sources of sediments for this unit. These source areas are located in the basement of the Amagá Basin and/or in the adjacent cordilleras (Silva et al., 2008; Sierra and Marín-Cerón, 2011). However, Lara et al. (2015) and Montes et al. (2015) suggest, through U—Pb data of detrital zircons that the Upper Member of the Amagá Formation has source areas outside of the South American plate, with a probable early to middle-Miocene land connection between the Panama-Choco Block (PCB) and the Northern Andean Block (NAB). Our magnetic mineralogy results characterize changes in the source areas between the Lower and Upper Member of the Amagá Formation. However, it is not conclusive for determining sediment input from the PCB to the Upper Member of the Amagá Formation. Changes in the magnetic mineralogy could also be related to erosional exhumation of rock massifs located within the NAB.

The Amagá Formation was affected by deformation during and after deposition (Van der Hammen, 1958; Sierra and Marín-Cerón, 2011). The deformation of this unit is also reflected by our magnetic fabric characterization. We characterized a sole site having pure sedimentary magnetic fabric, whilst the remaining sites possess intermediate magnetic fabrics (types II and III) and tectonic magnetic fabrics (types IV, V and VI) (Fig. 6b). The transition from sedimentary to intermediate or tectonic magnetic fabrics is a process which involves the reorientation of the principal magnetic fabric elements. The magnetic lineations and magnetic foliations gradually deviates from their original sedimentary-related directions, showing deformation in different structural regimes (Kligfield et al., 1983; Sagnotti et al., 1994; Mattei et al., 1997; Cifelli et al., 2005; Chadima et al., 2006; Soto et al., 2009; Oliva-Urcia et al., 2013; García-Lasanta et al., 2014).

The Amagá Formation was deposited in a transpressive structural context linked to the subduction of the Farallon-Nazca Plate, the accretion of tectonic blocks and terranes to the northwestern margin of South America and the strike-slip behavior of the Cauca-Romeral fault system (Sierra and Marín-Cerón, 2011). Mean magnetic lineations of the different sampled successions are mainly oriented in NE-SW directions. Although the mean magnetic lineations of the Albania and Palomos sections are oriented in NE-SW directions (Fig. 7), these successions have high confidence angles for their magnetic fabric principal directions. This fact is probably linked to the paramagnetic minerals which control the magnetic fabrics of these successions. On the other hand, the Excarbon, Venecia and Crisol sections show good trends of their magnetic lineations with NE-SW directions. The Cinco section slightly differs from the other sections and has some specimens with E-W oriented magnetic lineations (Fig. 7). Considering the regional structural context, we suggest that the rotation of the magnetic lineations is linked to a compressional event perpendicular to the orientation of the magnetic lineations (Kligfield et al., 1983; Mattei et al., 1997; Chadima et al., 2006; Soto et al., 2009). Thereby, a NW-SE compressional direction strain (bed-parallel shortening) can be identified. The PCB was accreted in E-SE direction to northwestern South America (Duque-Caro, 1990; Cortés and Angelier, 2005; Suter et al., 2008). Therefore, the compressional strain is most likely related with the PCB collision against the NAB and the influence of this event under the western area of the South American Plate, since the late Oligocene (Farris et al., 2011; O'Dea et al., 2016).

The NW-SE compression is compensated by an NE-SW extension. This deformation mechanism involves a simple shear system, which is

related to the Cauca-Romeral strike-slip fault system (MacDonald, 1980; Sierra, 1994; MacDonald et al., 1996; Chicangana, 2005; Sierra et al., 2012). NW-SE compression in this transpressive context has also been documented in other areas of the Cauca depression (Cortés and Angelier, 2005; Suter et al., 2008).

It is hard to distinguish between the influence of bed-parallel shortening and/or simple shear using magnetic fabrics. Both behaviors involve a re-orientation of the magnetic lineations, which can be sub-horizontal or sub-vertical in a transpressive stress-regime (Ježek and Hrouda, 2002) and sub-vertical if lateral shortening is predominant (Chadima et al., 2006). On the other hand, the magnetic foliations tend to be sub-vertical (Chadima et al., 2006). This is not the case of the magnetic fabrics of the Amagá Formation. The magnetic lineations are well re-oriented with sub-horizontal inclinations, however, the magnetic foliations are usually sub-horizontal. The well re-orientated magnetic lineation, the sub-horizontal magnetic foliations and the presence of intermediate magnetic fabrics are evidences of some early stages of deformation, which are concordant with a NW-SE compression direction. The Venecia section, which constitutes the first deposited succession of the Upper Member of the Amagá Formation, has strongly oblate AMS ellipsoids, which are usually difficult to be overprinted by bed-parallel shortening and/or simple shear (Chadima et al., 2006). However, the magnetic lineations of the intermediate magnetic fabrics type II of the Venecia section are well-reoriented perpendicular to the compression direction. Under the deformational regime of the Amagá Formation, a good reorientation of the magnetic lineations, after the compaction of sediments, would have involved a change from magnetic fabrics type II to intermediate magnetic fabrics type III or tectonic magnetic fabrics, as it is observed in the Cinco and Crisol sections (Table 2; Fig. 6b). There the loss of the sedimentary signature of the magnetic fabrics (high *f* angles) is accompanied by a reorientation of the magnetic lineations. Thereby, we suggest that the magnetic fabrics of the Venecia section deposits were acquired during deformational events coeval with the earliest diagenesis stages of the sediments, which had a high amount of vertical compaction (Fig. 9b).

Syndepositional deformation occurred between ~28 Ma and ~17 Ma, based on the age constraints we have for the Lower and Upper members of the Amagá Formation (Table 1). However, the syndepositional deformation of the Upper Member of the Amagá Formation may have started with the first accretionary event of the PCB against the NAB (25–21 Ma; Farris et al., 2011; Farris et al., 2017).

Deformation after deposition/compaction of the Amagá Formation is evidenced by the re-orientation of the magnetic lineations and the prolate to neutral AMS ellipsoids of fabrics type III and type IV of the Excarbon succession (Lower Member of the Amagá Formation) (Fig. 9b). Deformational events during the deposition/compaction of the Lower Member of the Amagá Formation could not be identified. Our observations only show that the Lower Member of the Amagá Formation was deformed after deposition in the transpressive stress-field of the Amagá Basin (Fig. 9a). The stratigraphically youngest deposits of the Upper Member of the Amagá Formation (Crisol and Cinco sections) also present deformation after compaction (Fig. 9d). This is evidenced by magnetic fabrics type III, IV and V with well re-oriented magnetic lineations and a gradual loss of the sedimentary signature. These successions could also be affected by syndepositional deformation, which was linked to collisional stages of the PCB against the NAB. However, a low amount of vertical compaction, over the Crisol and Cinco successions, allows a good re-orientation of the magnetic fabrics of these successions (Fig. 9c, d).

The Venecia section deposits is also affected by deformation after deposition/compaction. This can be related with the Quaternary strain of the PCB against the NAB (Cortés and Angelier, 2005; Suter et al., 2008; O'Dea et al., 2016). However, the strongly oblate AMS ellipsoids, acquired during the diagenesis of the rocks of the Venecia section, are difficult to be overprinted. Furthermore, the deformational events which affected the Venecia section during and after its deposition/compaction was similar in terms of compressional direction and behavior, such as it is evidenced by the NE-SW magnetic directions of the other sections (Fig. 7).

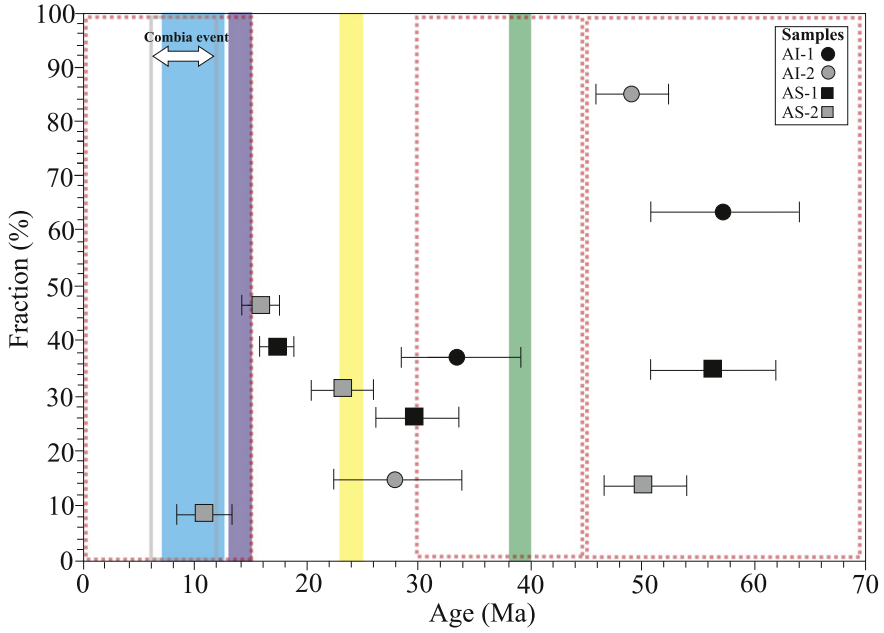

Fig. 8. Correlation between zircon fission-track peak ages (2σ errors) of the Amagá Formation, the fraction of grains in each peak and the timing of different geological events recorded in the Northern Andes. Regional exhumation events are shown by red dotted lines (Villagómez and Spikings, 2013). The green band indicates the accretion of an oceanic terrane to the western margin of the NAB (Kerr et al., 1997; Cediel et al., 2003; Echeverry et al., 2015). The yellow band shows the initiatial accretionary event of the PCB against the NAB (Farris et al., 2011). Montes et al. (2015) defines a final accretionary event of the PCB at ~15–13 Ma (purple band). However, Coates et al. (2004) proposed ~11–7 Ma collisional stages of the PCB against the NAB (blue band). The gray lines limit the age of the volcanic Combia event (Leal-Mejía, 2011).

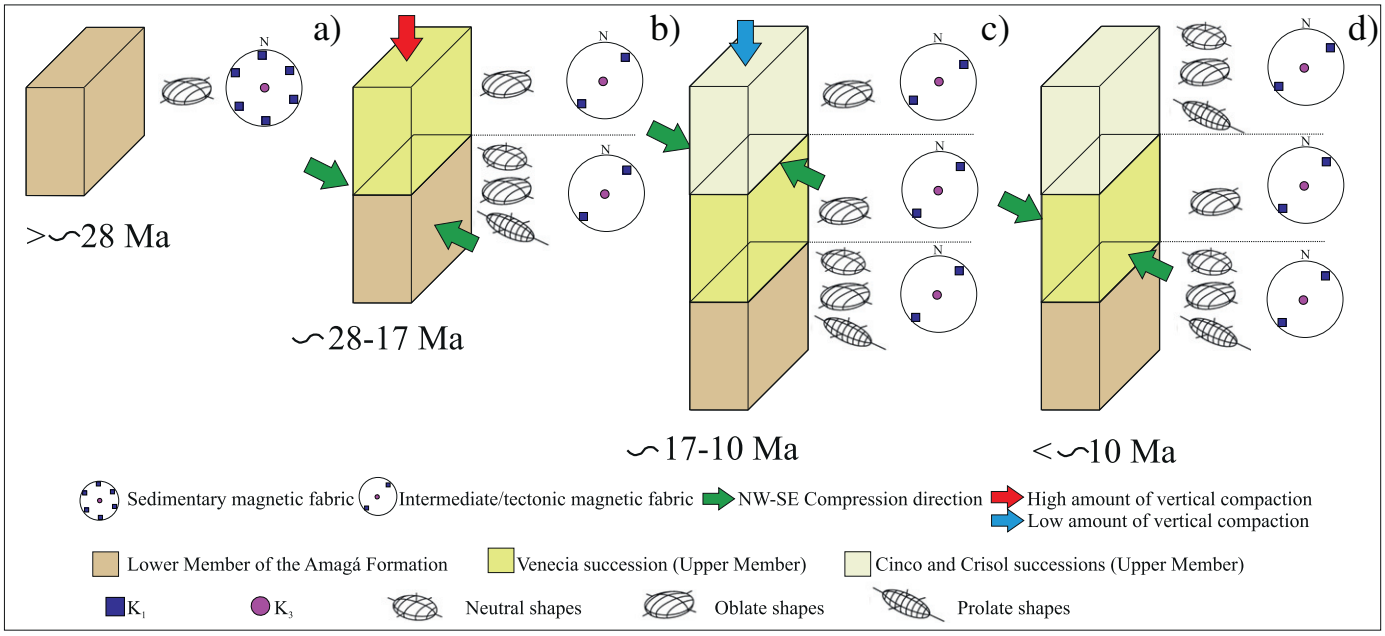

Fig. 9. Schematic model of the deformation of the Amagá Formation. (a) Deposition of the Lower Member of the Amagá Formation. (b) Syntectonic deposition of the Venecia succession and deformation of the Lower Member of the Amagá Formation. At this stage, a high amount of vertical compaction is characterized. (c) Syntectonic deposition of the Cinco and Crisol successions. At this stage, a low amount of vertical compaction was characterized. (d) Post-consolidation deformation of the Amagá Formation.

5.3. Geodynamic and tectonic implications

The ZFT ages of the Amagá Formation record cooling in the northern Andes, most likely related to erosional exhumation. Late Paleocene to early Eocene detrital ZFT cooling ages (Table 1) are compatible with orogenic evolution of the Northern Andes determined in stratigraphical and thermochronological studies (Van der Hammen, 1958; Restrepo-Moreno et al., 2009; Parra et al., 2009a; Villagómez and Spikins, 2013). This evolution is mainly related to the subduction of the Farallon-Nazca Plate beneath the South American Plate, after the collision of the Caribbean Large Igneous Province with northern South America (Villagómez and Spikins, 2013). The western margin of the Northern Andean Block (NAB) was also affected by late Eocene accretionary events (Kerr et al., 1997; Cediel et al., 2003; Echeverri et al., 2015), which may have caused Eocene-early Oligocene exhumational cooling in the Western and Central Cordilleras of Colombia. Similarly, further south in the Andean chain, in Ecuador, Peru and Bolivia continuous exhumation between ~45 and ~30 Ma has been recorded (Mégard, 1984; Barnes et al., 2006; Spikings et al., 2010). In Colombia, such exhumation has been documented in several areas of the Cordilleras and in the the Magdalena River valley sedimentary deposits (Villamil, 1999; Restrepo-Moreno et al., 2009; Parra et al., 2009a; Villagómez and Spikins, 2013). Early Oligocene ZFT ages of the the Amagá Formation (33.7 ± 5.5, 29.8 ± 3.8 and 28.1 ± 5.8) are new markers of the ~45–30 Ma regional exhumation pulse within the Andean chain (Fig. 8).

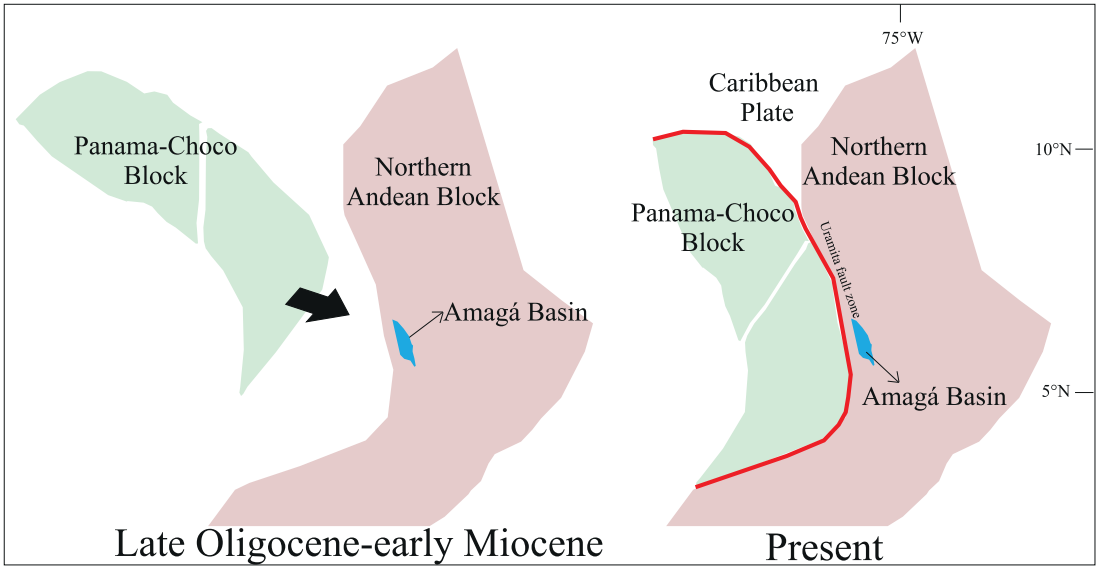

Fig. 10. Schematic model of the PCB collision with the NAB. The collisional stages between these tectonic blocks may have started during the Late Oligocene-early Miocene.

Late Oligocene to middle Miocene exhumation is known from the Central Andes of South America (Mégard, 1984; Gregory-Wodzicki, 2000; Barnes et al., 2006; Spikings et al., 2010) and some regions of the northern Andes (Parra et al., 2009a; Villagómez et al., 2011; Amaya et al., 2017). This late Oligocene-early Miocene exhumation in the northern Andes involves complex geological events such as the split of the Farallon Plate and the accretion of the Panama-Choco Block (PCB) to the Northern Andean Block (NAB) (Lonsdale, 2005; Farris et al., 2011; Villagómez and Spikings, 2013). Far-field effects of the PCB accretion have been recorded in fast exhumation at ~25 Ma on the western flank of the Santander Massif of the Eastern Cordillera, and accelerated exhumation between 25 and 21 Ma in Antioquia Batholith in the Central Cordillera of Colombia (Restrepo-Moreno, 2009). We present a late Oligocene-early Miocene ZFT age of 22.9 ± 2.8 in the Upper Member of the Amagá Formation, which may be linked to the first accretionary event of the PCB to northwestern South America between 25 and 21 Ma (Fig. 8; Farris et al., 2011; Farris et al., 2017).

We also present Miocene ZFT ages of 17.6 ± 1.6, 15.5 ± 1.6 which can be related to a regional exhumation event in the northern Andes. This event is linked to the collision of the Carnegie Ridge (Villagómez and Spikings, 2013) and continuous Miocene collisional stages of the PCB to northwestern South America (Fig. 8).

Therefore, within the NAB, the PCB collision is reflected by exhumation of rock massifs (Farris et al., 2011) and changes in the sedimentary environments and source areas of the Amagá Formation (Lara et al., 2015; Montes et al., 2015). Our magnetic fabric results show that the Upper Member of the Amagá Formation was deposited during periods of intense tectonic activity, which deformed this unit during and partly after its deposition/compaction. The NE-SW trend of the magnetic lineations show that the deformation of the Amagá Basin is closely related to the PCB collision and its NW-SE σ_1 within the Cauca depression (Suter et al., 2008). Therefore, we consider that the influence of the PCB over the Amagá Formation started with the 25–21 first collisional stage of the PCB against the NAB (Farris et al., 2011; Farris et al., 2017). During and after deposition/compaction, the deformation of the Amagá Formation was linked to continuous collisional stages of the PCB (Fig. 10).

6. Conclusions

The Lower Member of the Amagá Formation is an Oligocene sedimentary succession which records late Paleocene to late Oligocene exhumation events in the northern Andes. The source areas of the Lower Member of the Amagá Formation are located in the basement rocks of the Central and Western Cordilleras of Colombia, adjacent to the Amagá Basin. The middle-Miocene Upper Member of the Amagá Formation recorded Miocene exhumation of the Northern Andean Block (NAB). The regionally most pertinent exhumation was driven by the collision of the Panama-Choco Bloc (PCB) with the NAB at 25–21 Ma. The source areas of the sediments of the Upper Member of the Amagá Formation are also found in the Central and Western Cordilleras of Colombia.

The Lower Member of the Amagá Formation was deformed by the same deformational events which affected the Upper Member. The Upper Member of the Amagá Formation was affected by both *syn*- and post-depositional/compaction deformation. The deformation of the Amagá Formation is related to the regional stress-field, including bed-parallel shortening in NW-SE direction and NE-SW simple shear. The deformation observed in the Amagá Basin and other regions of the Cauca depression (e.g. Cortés and Angelier, 2005; Suter et al., 2008), is linked to the subduction of the Farallon-Nazca Plate beneath the South American plate, the strike-slip faults of the Cauca-Romeral fault system and the collisional stages of the PCB against the NAB.

Acknowledgements

This project is supported by the programs Jóvenes investigadores e innovadores (Convocatoria 706-2015-Colciencias-Víctor Andrés Piedrahita) and ECOS-Nord – COLCIENCIAS-ICETEX grants C12U01 and C16U01. Suggestions by two anonymous reviewers greatly improved the final version of the manuscript.

Appendix A. Supplementary data

Supplementary data to this article can be found online at http://dx.doi.org/10.1016/j.sedgeo.2017.05.003.

References

Acosta, C.A., 1978. El graben interandino Colombo-Ecuatoriano (Fosa Tectónica del Cauca Patía y el corredor Andino-Ecuatoriano). Boletín de Geología Universidad Industrial de Santander 12, 63–75.

Alfonso, C.A., Sacks, P.E., Secor, D.T., Rine, J., Perez, V., 1994. A tertiary fold and thrust belt in the Valle del Cauca Basin, Colombian Andes. Journal of South American Earth Sciences 7, 387–402.

Amaya, S., Zuluaga, C.A., Bernet, M., 2017. New fission-track age constraints on the exhumation of the central Santander Massif: implications for the tectonic evolution of the Northern Andes, Colombia. Lithos 282-283, 388–402.

Archanjo, C.J., da Silva, E.R., Caby, R., 1999. Magnetic fabric and emplacement in a transpressive shear zone system: the Itaporanga porphyritic granite pluton (northeast Brazil). Tectonophysics 312, 331–345.

Arrubla, O.H., 2012. Zonificación del potencial de gas asociado al carbón y sus controles geológicos en la cuenca carbonífera de Amagá. Tesis de pregrado. Universidad EAFIT, Medellin, Colombia.

Aubourg, C., Smith, B., Bakhtari, K., Guya, N., Eshragi, A., Lallemant, S., Molinaro, M., Braud, X., Delaunay, S., 2004. Post-Miocene shortening pictured by magnetic fabric across the Zagros-Makran syntaxix (Iran). In: Sussman, A.J., Weil, A.B. (Eds.), Orogenic Curvature: Integrating Paleomagnetic and Structural Analyses. Boulder, Colorado. Geological Society of America Special Papers vol. 383, pp. 17–40.

Averbuch, O., Lamotte, D.F., Kissel, C., 1992. Magnetic fabric as a structural indicator of the deformation path within a fold-thrust structure: a test case from the Corbieres (NE Pyrenees, France). Journal of Structural Geology 14, 461–474.

Balsley, J.R., Buddington, A.F., 1960. Magnetic susceptibility anisotropy and fabric of some Adirondack granites and orthogneisses. American Journal of Science 258A, 6–20.

Barnes, J.B., Ehlers, T.A., McQuarrie, N., O'Sullivan, P.B., Pelletier, J.D., 2006. Eocene to recent variations in erosion across the central Andean fold-thrust belt, northern Bolivia: implications for plateau evolution. Earth and Planetary Science Letters 248, 118–133.

Barrero, D., Pardo, A., Vargas, C.A., Martinez, J.F., 2007. Colombian Sedimentary Basins: Nomenclature, Boundaries and Petroleum Geology, A New Proposal. ANH and B&M Exploration Ltda, Bogotá, Colombia.

Bernet, M., 2009. A field-based estimate of the zircon fission-track closure temperature. Chemical Geology 259 (3), 181–189.

Bernet, M., Garver, J.I., 2005. Fission-track dating of detrital zircon. In: Reiners, P., Ehlers, T. (Eds.), Thermochronology. Reviews in Mineralogy and Geochemistry vol. 58, pp. 205–238.

Bernet, M., Brandon, M.T., Garver, J.I., Molitor, B.R., 2004. Fundamentals of detrital zircon fission-track analysis for provenance and exhumation studies with examples from the European Alps. Geological Society of America Special Papers 378, 25–36.

Bernet, M., van der Beek, P., Pik, R., Huyghe, P., Mugnier, J.L., Labrin, E., Szulc, A., 2006. Miocene to recent exhumation of the central Himalaya determined from combined detrital zircon fission-track and U/Pb analysis of Siwalik sediments, western Nepal. Basin Research 18 (4), 393–412.

Bernet, M., Brandon, M., Garver, J., Balestieri, M.L., Ventura, B., Zattin, M., 2009. Exhuming the Alps through time: clues from detrital zircon fission-track thermochronology. Basin Research 21 (6), 781–798.

Blanco-Quintero, I.F., García-Casco, A., Toro, L.M., Moreno, M., Ruiz, E.C., Vinasco, C.J., Cardona, A., Lázaro, C., Morata, D., 2014. Late Jurassic terrane collision in the northwestern margin of Gondwana (Cajamarca complex, eastern flank of the Central Cordillera, Colombia). International Geology Review 56 (15):1852–1872. http://dx.doi.org/10.1080/00206814.2014.963710.

Borradaile, G.J., 1988. Magnetic susceptibility, petrofabrics and strain. Tectonophysics 156, 1–20.

Borradaile, G.J., 2001. Magnetic fabrics and petrofabrics: their orientation distributions and anisotropies. Journal of Structural Geology 23, 1581–1596.

Borradaile, G.J., Jackson, M., 2010. Structural geology, petrofabrics and magnetic fabrics (AMS, AARM, AIRM). Journal of Structural Geology 32, 1519–1551.

Brandon, M.T., 2002. Decomposition of mixed grain age distributions using BinomFit. On Track 24, 13–18.

Brandon, M.T., Roden-Tice, M.K., Garver, J.I., 1998. Late Cenozoic exhumation of the Cascadia accretionary wedge in the Olympic Mountains, northwest Washington State. Geological Society of America Bulletin 110 (8), 985–1009.

Buchs, D.M., Arculus, R.J., Baumgartner, P.O., Ulianov, A., 2011. Oceanic intraplate volcanoes exposed: example from seamounts accreted in Panama. Geology 39 (4): 335–338. http://dx.doi.org/10.1130/G31703.1.
Calle, B. and González, H. 1980. Geología y geoquímica de la plancha 166, Jericó Escala 1: 100000, Memoria explicativa. Ingeominas, Bogotá, Colombia.
Calle, B., González, H., de La Peña, D., Escorce, E., Durango, M and others. 1980. Geología de la Plancha 166 Jericó, Escala 1:100000. Ingeominas, Bogotá, Colombia.
Callot, J.P., Robion, P., Sassi, W., Guiton, M.L.E., Faure, J.-L., Daniel, J.M., Mengus, J.M., Schmitz, M., 2010. Magnetic characterization of folded aeolian sandstones: interpretation of magnetic fabrics in diamagnetic rocks. Tectonophysics 495, 230–245.
Case, J.E., Duran, L.G., López, A., Moore, W.R., 1971. Tectonic investigations in Western Colombia and Eastern Panama. Geological Society of America Bulletin 82, 2685–2712.
Cediel, F., Shaw, R.P., Cáceres, C., 2003. Tectonic assembly of the Northern Andean Block. In: Bartolini, C., Buffler, R., Blickwede, J. (Eds.), The Circum-Gulf of México and Caribbean: Hydrocarbon Habitats, Basin Formation and Plate Tectonics. American Association of Petroleum Geologists vol. 79, pp. 815–848.
Chadima, M., Jelinek V., 2009. Anisoft 4.2. Anisotropy data browser for Windows. Agico, Inc.
Chadima, M., Hrouda, F., Melichar, R., 2006. Magnetic fabric study of the SE Rhenohercynian Zone (Bohemian Massif): implications for dynamics of the Paleozoic accretionary wedge. Tectonophysics 418 (1–2):93–109. http://dx.doi.org/10.1016/j.tecto.2005.12.015.
Chicangana, G., 2005. The Romeral fault system: a shear and deformed extinct subduction zone between oceanic and continental lithospheres in Northwestern South America. Earth Science Research 9 (1), 51–66.
Cifelli, F., Mattei, M., Chadima, M., Hirt, A.M., Hansen, A., 2005. The origin of tectonic lineation in extensional basins: combined neutron and magnetic analyses on "undeformed" clays. Earth and Planetary Science Letters 235, 62–78.
Coates, A.G., Collins, L.S., Aubry, M.P., Berggren, W.A., 2004. The geology of the Darien, Panama, and the Miocene-Pliocene collision of the Panama arc with northwestern South America. Geological Society of America Bulletin 116 (11), 1327–1344.
Cortés, M., Angelier, J., 2005. Current states of stress in the northern Andes as indicated by focal mechanisms of earthquakes. Tectonophysics 403 (1–4):29–58. http://dx.doi.org/10.1016/j.tecto.2005.03.020.
de Boer, J.Z., Defant, M.J., Stewart, R.H., Bellon, H., 1991. Evidence for active subduction below western Panama. Geology 19 (6):649–652. http://dx.doi.org/10.1130/0091–7613(1991)019<0649:EFASBW>2.3.CO;2.
Duque-Caro, H., 1990. The Choco block in the northwestern corner of South America: structural, tectonostratigraphic, and paleogeographic implications. Journal of South American Earth Sciences 3, 71–84.
Echeverri, S., Cardona, A., Pardo-Trujillo, A., Borrero, C., Rosero, S., López, S., 2015. Correlación y geocronología Ar-Ar del basamento Cretácico y el relleno sedimentario Eoceno Superior - Mioceno (Aquitaniano inferior) de la cuenca de antearco de Tumaco, SW de Colombia. Revista Mexicana de Ciencias Geológicas 32 (2), 179–189.
Ego, F., Sébrier, M., 1995. Is the Cauca-Patía and Romeral Fault System left or right-lateral? Geophysical Research Letters 22 (1), 33–36.
Farris, D.W., Jaramillo, C., Bayona, G., Restrepo-Moreno, A., Montes, C., Cardona, A., Mora, A., Speakman, R.J., Glascock, M.D., Valencia, V., 2011. Fracturing of the Panamanian Isthmus during initial collision with South America. Geology 39, 1007–1010.
Farris, D.W., Cardona, A., Montes, C., Foster, D., Jaramillo, C., 2017. Magmatic evolution of Panama Canal volcanic rocks: a record of arc processes and tectonic change. PloS One 12 (5), e0176010. http://dx.doi.org/10.1371/journal.pone.0176010.
Fleischer, R.L., Price, P.B., Walker, R.M., 1975. Nuclear Tracks in Solids Principles and Applications. University of California Press.
Galbraith, R.F., 1981. On statistical models for fission-tracks counts. Mathematical Geosciences 13:471–478. http://dx.doi.org/10.1007/BF01034498.
Galbraith, R.F., Green, P.F., 1990. Estimating the component ages in a finite mixture. International Journal of Radiation Applications and Instrumentation. Part D. Nuclear Tracks and Radiation Measurements 17 (3), 197–206.
Galbraith, R.F., Laslett, G.M., 1993. Statistical models for mixed fission track ages. Nuclear Tracks and Radiation Measurements 21 (4), 459–470.
Gallagher, K., Brown, R., Johnson, C., 1998. Fission track analysis and its application to geological problems. Annual Review of Earth and Planetary Sciences 26, 519–572.
Gansser, A., 1973. Facts and theories on the Andes. Journal of the Geological Society 129, 93–131.
García-Lasanta, C., Oliva-Urcia, B., Román-Berdiel, T., Casas, A.M., Hirt, A.M., 2014. Understanding the Mesozoic kinematic evolution in the Cameros basin (Iberian Range, NE Spain) from magnetic subfabrics and mesostructures. Journal of Structural Geology 66, 84–101.
Gleadow, A.J.W., 1981. Fission track dating methods: what are the real alternatives? Nuclear Tracks 5, 3–14.
González, H., 2001. Mapa geológico del departamento de Antioquia. Geología, recursos minerales y amenazas potenciales, Escala 1:400000, Memoria explicativa. Ingeominas, Bogotá, Colombia.
González, H., Nuñez, A., Paris, G., 1988. Mapa Geológico de Colombia. Memoria explicativa. Ingeominas, Bogotá. Colombia.
Graham, J.W., 1966. Significance of magnetic anisotropy in Appalachian sedimentary rocks. In: Steinhart, J.S., Smith, T.J. (Eds.), The Earth Beneath the Continents. American Geophysical Union, Geophysical Monograph Series vol. 10, pp. 627–648.
Grégoire, V., de Saint Blanquat, M., Nédélec, A., Bouchez, J.L., 1995. Shape anisotropy versus magnetic interactions of magnetite grains: experiments and application to AMS in granitic rocks. Geophysical Research Letters 22 (20), 2765–2768.
Gregory-Wodzicki, K.M., 2000. Uplift history of the central and Northern Andes: a review. Geological Society of America Bulletin 112, 1091–1105.
Grosse, E., 1926, Mapa geológico de la parte occidental de la Cordillera Central entre el río Arma y Sacaojal, 1:50000, el terciario Carbonífero de Antioquia, Berlin, Germany.
Hamilton, N., Rees, A.I., 1970. Magnetic fabric of sediments from the shelf at La Jolla (California). Marine Geology 9, 6–11.
Henao-Betancur, J., 2012. Estratigrafía y petrografía de las areniscas de la secuencia quebrada la Naranjala-Municipio de Fredonia Miembro inferior de la Formación Amagá. Proyecto de grado, Universidad Eafit, Medellín, Colombia.
Hernández, I.E., 1999. Petrología de las areniscas de la sección Peñitas-Mina Excarbon, Miembro medio de la Formación Amagá, Titiribí-Antioquia. Tesis de maestría. Universidad Eafit, Medellín, Colombia.
Hirt, A.M., Lowrie, W., Lüneburg, C., Lebit, H., Engelder, T., 2004. Magnetic and mineral fabric development in the Ordovician Martinsburg formation in the central Appalachian fold and Thrust Belt, Pennsylvania. In: Martín-Hernández, F., Lünburg, C., Auboug, C., Jackson, M. (Eds.), Magnetic Fabric: Methods and Applications. Geological Society of London, Special Publication vol. 238, pp. 109–126.
Hrouda, F., 1982. Magnetic anisotropy of rocks and its application in geology and geophysics. Geophysical Surveys 5, 37–82.
Hrouda, F., 1994. A technique for the measurement of thermal changes of magnetic susceptibility of weakly magnetic rocks by the CS-2 apparatus and KLY-2 Kappabridge. Geophysical Journal International 118, 604–612.
Hrouda, F., Jelinek, V., Zapletal, K., 1997. Refined technique for susceptibility resolution into ferromagnetic and paramagnetic components based on susceptibility temperature-variation measurement. Geophysical Journal International 129, 715–719.
Hurford, A.J., Carter, A., 1991. The role of fission track dating in discrimination of provenance. In: Morton, A., Todd, S. (Eds.), Developments in Sedimentary Provenance Studies. Geological Society, London, Special Publication vol. 57, pp. 67–78.
Hurford, A.J., Green, P.F., 1983. The zeta calibration of fission track dating. Isotope Geoscience 1, 285–317.
Hutchings, L., Turcotte, T., McBride, J., Ochoa, H., 1981. Microseismicity along and near the Dolores Shear Zone in Antioquia, Colombia. Revista CIAF 6 (1–3). pp. 243–256.
Jelinek, V., 1977. The Statistical Theory of Measuring Anisotropy of Magnetic Susceptibility of Rocks and Its Application. Geofyzika, Brno.
Jelinek, V., 1981. Characterization of the magnetic fabric of rocks. Tectonophysics 79, 63.
Ježek, J., Hrouda, F., 2002. Software for modeling the magnetic anisotropy of strained rocks. Computers and Geosciences 28, 1061–1068.
Kammer, A., 1993. Las fallas de Romeral y su relación con la tectónica de la Cordillera Central. Geología Colombiana 18, 27–46.
Kerr, A.C., Marriner, G.F., Tarney, J., Nivia, A., Saunders, A.D., Thirlwall, M.F., Sinton, C.W., 1997. Cretaceous basaltic terranes in Western Columbia: elemental, chronological and Sr–Nd isotopic constraints on petrogenesis. Journal of Petrology 38, 677–702.
Kligfield, R., Lowrie, W., Hirt, A.M., Siddans, A.W.B., 1983. Effect of progressive deformation on remanent magnetization of Permian red beds from the Maritime Alps (France). Tectonophysics 97, 59–85.
Lara, M.E., Silva, J.C., Salazar, A.M., 2015. Early Miocene Accretion of Panamá to Northern South America. Sedimentologic and Geochronologic Evidence From an Intramontane Siliciclastic Succession in the Northwestern Andes. Goldschmidt Conference Abstracts. p. 1675.
Leal-Mejía, H., 2011. Phanerozoic gold metallogeny in the Colombian Andes: a tectono-magmatic approach. PhD Thesis. Universitat de Barcelona, Barcelona, Spain.
Lonsdale, P., 2005. Creation of the Cocos and Nazca plates by fission of the Farallon plate. Tectonophysics 404, 237–264.
Lowrie, A., Stewart, J.L., Stewart, R.H., Van Andel, T.J., McRaney, L., 1982. Location of the eastern boundary of the Cocos Plate during the Miocene. Marine Geology 45 (3–4): 261–279. http://dx.doi.org/10.1016/0025-3227(82) 90114-1.
MacDonald, W.D., 1980. Anomalous paleomagnetic directions in the Late Tertiary andesitic intrusions of the Cauca Depression, Colombian Andes. Tectonophysics 68, 339–348.
MacDonald, W.D., Estrada, J., Sierra, G., González, H., 1996. Late Cenozoic tectonics and paleomagnetism of North Cauca Basin intrusions, Colombian Andes: dual rotation modes. Tectonophysics 261, 277–289.
Mann, P., Corrigan, J., 1990. Model for late Neogene deformation in Panama. Geology (Boulder) 18, 558–562.
Mann, P., Kolarsky, R.A., 1995. East Panama deformed belt: structure, age, and neotectonic significance. In: Mann, P. (Ed.), Geologic and Tectonic Development of the Caribbean Plate Boundary in Southern Central America. Journal of Geophysical Research, Boulder, Colo., pp. 111–130.
Mattei, M., Sagnotti, L., Faccenna, C., Funiciello, R., 1997. Magnetic fabric of weakly deformed clay-rich sediments in the Italian peninsula: relationship with compressional and extensional tectonics. Tectonophysics 271, 107–122.
Maya, M., González, H., 1995. Unidades Litodémicas de la Cordillera Central de Colombia. Boletín Geológico de Ingeominas 35 (2–3), 43–57.
Mégard, F., 1984. The Andean orogenic period and its major structures in central and northern Peru. Journal of the Geological Society of London 141, 893–900.
Mejía, M., James, M., Arias, L.A., 1988. Evaluación de amenazas geológicas en el área Manizales - Valparaíso. Ingeominas, Medellín, Colombia.
Mesa-García, J., 2015. Combia Formation: A Miocene Immature Volcanic Arc? Master Thesis. Eafit University, Medellín, Colombia.
Montes, C., Hatcher, R.D., Restrepo-Pace, P.A., 2005. Tectonic reconstruction of the northern Andean blocks: oblique convergence and rotations derived from the kinematics of the Piedras-Girardot area, Colombia. Tectonophysics 399:221–250. http://dx.doi.org/10.1016/j.tecto.2004. 12.024.
Montes, L.F., 2007. Exhumación de las rocas metamórficas de alto grado que afloran al oriente del valle del Aburrá, Antioquia. Tesis de maestría. Universidad EAFIT 124 p. Medellín.
Montes, C., Cardona, A., McFadden, R., Morón, S.E., Silva, C.A., Restrepo-Moreno, S., Ramírez, D.A., Hoyos, N., Wilson, J., Farris, D., 2012. Evidence for Middle Eocene and

younger land emergence in central Panama: implications for Isthmus closure. Geological Society of America Bulletin 124, 780–799.
Montes, C., Cardona, A., Jaramillo, C., Pardo, A., Silva, J.C., Valencia, V., Ayala, C., Pérez-Angel, L.C., Rodriguez-Parra, L.A., Ramirez, V., Niño, H., 2015. Middle Miocene closure of the Central American Seaway. Science 348, 226–229.
Mora, A., Casallas, W., Ketcham, R.A., Gomez, D., Parra, M., Namson, J., Stockli, D., Almendral, A., Robles, W., Ghorbal, B., 2015. Kinematic restoration of contractional basement structures using thermokinematic models: a key tool for petroleum system modeling. American Association of Petroleum Geologists Bulletin 99:1575–1598. http://dx.doi.org/10.1306/04281411108.
Moreno-Quimbay, N., 2011. Análisis de la petrología, área fuente y diagenesis de las areniscas de la Formación Amagá en los pozos Venecia 1 y el Cinco (1B). Proyecto de grado. Universidad Eafit, Medellín, Colombia.
Murillo, S., 1998. Petrografía de las areniscas de la secuencia Quebrada la Sucia- Mina Palomos, Miembro Inferior de la Formación Amagá. Proyecto de Grado. Universidad Eafit, Medellín, Colombia.
Nagaraju, J., Chetty, T.R.K., Vara Prasad, G.S., Patil, S.K., 2008. Transpressional tectonics during the emplacement of Pasupugallu Gabbro Pluton, Western margin of Eastern Ghats Mobile Belt, India: evidence from AMS fabrics. Precambrian Research 162 (1–2):86–101 ISSN 0301-9268. 10.1016/j.precamres.2007.07.025.
Nagata, T., 1961. Rock Magnetism. second ed Maruzen, Tokyo, Japan.
O'Dea, A., Lessios, H.A., Coates, A.G., Eytan, R.I., Restrepo-Moreno, S.A., Cione, A.L., Collins, L.S., de Queiroz, A., Farris, D.W., Norris, R.D., Stallard, R.F., Woodburne, M.O., Aguilera, O., Aubry, M., Berggren, W.A., Budd, A.F., Cozzuol, M.A., Coppard, S.E., Duque-Caro, H., Finnegan, S., Gasparini, G.M., Grossman, E.L., Johnson, K.G., Keigwin, L.D., Knowlton, N., Leigh, E.G., Leonard-Pingel, J.S., Marko, P.B., Pyenson, N.D., Rachello-Dolmen, P.G., Soibelzon, E., Soibelzon, L., Todd, J.A., Vermeij, G.J., Jackson, J.B.C., 2016. Formation of the Isthmus of Panama. Science Advances 2. http://dx.doi.org/10.1126/sciadv.1600883.
Oliva-Urcia, B., Román-Berdiel, T., Casas, A.M., Bógalo, M.F., Osácar, M.C., García-Lasanta, C., 2013. Transition from extensional to compressional magnetic fabrics in the Cretaceous Cabuérniga basin (North Spain). Journal of Structural Geology 46, 220–234.
Parés, J.M., van der Pluijm, B.A., Dinarès-Turell, J., 1999. Evolution of magnetic fabrics during incipient deformation of mudrocks (Pyrenees, Northern Spain). Tectonophysics 307, 1–14.
Parra, M., Mora, A., Sobel, A.E., González, R., 2009a. Episodic orogenic front migration in the Northern Andes: constraints from low-temperature thermochronology in the Eastern Cordillera, Colombia. Tectonics 28, TC4004. http://dx.doi.org/10.1029/2008TC002423.
Parra, M., Mora, A., Jaramillo, C., Strecker, M.R., Sobel, E.R., Quiroz, L., Rueda, M., Torres, V., 2009b. Orogenic wedge advance in the Northern Andes: evidence from the Oligocene-Miocene sedimentary record of the Medina Basin, Eastern Cordillera, Colombia. Association of Petroleum Geologists Bulletin 121 (5–6):780–800. http://dx.doi.org/10.1130/B26257.1.
Pennington, W.D., 1981. Subduction of the eastern Panama Basin and seismotectonics of northwestern South America. Journal of Geophysical Research B 86, 10753–10770.
Pérez, A.M., 2013. Termocronología por huellas de fisión en apatitos de la Formación Amagá e intrusivos asociados (Pozos Venecia-1 y el Cinco-1B), Andes Colombianos. Proyecto de grado, Universidad Eafit, Medellín-Colombia.
Piedrahita, V.A., Molina-Garza, R.S., Sierra, G.M., Duque-Trujillo, J.D., 2017. Paleomagnetism and Magnetic Fabrics of Mio-Pliocene Hypabyssal Rocks of the Combia Event. Tectonic implications. Studia Geophisica et Geodaetica, Colombia http://dx.doi.org/10.1007/s11200-016-0372-0 (in press).
Price, P.B., Walker, R.M., 1963. Fossil tracks of charged particles in mica and the age of minerals. Journal of Geophysical Research 68, 4847–4862.
Pindell, J., Kennan, L., 2009. Tectonic evolution of the Gulf of Mexico, Caribbean and northern South America in the mantle reference frame: an update. Geological Society of London, Special Publication 328, 1–55.
Raposo, M.I.B., Berquó, T.S., 2008. Tectonic fabric revealed by AARM of the proterozoic mafic dike swarm in the Salvador City (Bahia State): São Francisco Craton, NE Brazil. Physics of the Earth and Planetary Interiors 167, 179–194.
Ramírez, E., Pardo-Trujillo, A., Plata, A., Vallejo, F., Trejos, R., 2015. Edad y ambiente de la Formación Amagá (Sector de Santa Fé de Antioquia-Sopetrán) con base en evidencias palinológicas. XV Congreso Colombiano de geología. Bucaramanga, Colombia, p. 277.
Reiners, P.W., Brandon, M.T., 2006. Using thermochronology to understand orogenic erosion. Annual Review of Earth and Planetary Sciences 34, 419–466.
Restrepo, J.J., Toussaint, J.F., González, H., 1981. Edades Mio-Pliocenas del magmatismo asociado a la Formación Combia, Departamentos de Antioquia y Caldas, Colombia. Geología Norandina 3, 22–26.
Restrepo-Moreno, S.A., Foster, D.A., Stockli, D.F., Parra-Sanchez, L.N., 2009. Long-term erosion and exhumation of the "Altiplano Antioqueno," Northern Andes (Colombia) from apatite (U-Th)/He thermochronology. Earth and Planetary Science Letters 278:1–12. http://dx.doi.org/10.1016/j.epsl.2008.09.037.
Restrepo, J.J., Toussaint, J.F., 1988. Terranes and continental accretion in the Colombian Andes. Episodes 7, 189–193.
Robion, P., Grelaud, S., de Lamotte, D.F., 2007. Pre-folding magnetic fabrics in fold-and-thrust belts: Why the apparent internal deformation of the sedimentary rocks from the Minervois basin (NE – Pyrenees, France) is so high compared to the Potwar basin (SW – Himalaya, Pakistan)? Sedimentary Geology 196, 181–200.
Rochette, P., 1987. Magnetic susceptibility of the rock matrix related to magnetic fabric studies. Journal of Structural Geology 9, 1015–1020.
Rochette, P., Jackson, J., Aubourg, C., 1992. Rock magnetism and the interpretation of ansisotropy of magnetic susceptibility. Reviews of Geophysics 30 (3), 209–226.
Rodríguez-Jimenez, V., 2010. Fábrica y emplazamiento de la Diorita de Pueblito, NW Cordillera Central de Colombia: análisis de fábrica magnética y mineral. Tesis de maestría. Universidad Nacional de Colombia, Medellín, Colombia.
Rodríguez, G., Arango, M.I., 2013. Reinterpretación geoquímica y radiométrica de las metabasitas del Complejo Arquía. Boletín de Geología 35 (2), 65–80.
Ruiz-Jiménez, E., Blanco-Quintero, I.F., Toro-Toro, L.M., Moreno-Sanchez, M., Vinasco, C.J., García-Casco, A., Morata, D., Gómez-Cruz, A., 2012. Geoquímica y petrología de las metabasitas del complejo arquía (municipio de Santafe de Antioquia y río Arquía, Colombia): implicaciones geodinámicas. Boletín de Ciencias de la Tierra 32, 65–80.
Sagnotti, L., Faccena, C., Funicello, R., Mattei, M., 1994. Magnetic fabric and structural setting of Plio-Pleistocene clayey units in an extensional regime: the Tyrrhenian margin of Central Italy. Journal of Structural Geology 16, 1243–1257.
Sierra, G.M., 1994. Structural and Sedimentary Evolution of the Irra Basin, Northern Colombian Andes. Master's Thesis. State University of New York, Binghamton, USA.
Sierra, G., Silva, J., Correa, L., 2004. Estratigrafía Secuencial de la Formación Amagá. Boletin de Ciencias de la Tierra 15, 9–22.
Sierra, G.M., Marín-Cerón, M.I., 2011. Amagá, Cauca and Patía Basins. In: Cediel, F. (Ed.), Petroleum Geology of Colombia, 2, Fondo Editorial Universidad Eafit, Medellín, Colombia.
Sierra, G.M., Marín-Cerón, M.I., MacDonald, 2012. Evolución tectónica de la Cuenca de tracción Irra. Evidencias de cambios en la zona de falla de Romeral, zona norte de la Cordillera Central de los Andes, Colombia. Boletín de Ciencias de la Tierra 32, 143–159.
Silva, J.C., Sierra, G.M., Correa, L.G., 2008. Tectonic and climate driven fluctuations in the stratigraphic base level of a Cenozoic continental coal basin, northwestern Andes. Journal of South American Earth Sciencies 26, 369–382.
Soto, R., Larrasoaña, J.C., Arlegui, L.E., Beamud, E., Oliva-Urcia, B., Simón, J.L., 2009. Reliability of magnetic fabric of weakly deformed mudrocks as a palaeostress indicator in compressive settings. Journal of Structural Geology 31, 512–522.
Spikings, R.A., Crowhurst, P.V., Winkler, W., Villagomez, D., 2010. Syn and post accretionary cooling history of the Ecuadorian Andes constrained by their in-situ and detrital thermochronometric record. Journal of South American Earth Sciences 30, 121–133.
Suter, F., Sartori, M., Neuwerth, R., Gorin, G., 2008. Structural imprints at the front of the Chocó-Panamá indenter: field data from the North Cauca Valley Basin, Central Colombia. Tectonophysics 460 (1–4):134–157. http://dx.doi.org/10.1016/j.tecto.2008.07.015.
Stacey, F.D., Joplin, G., Lindsay, J., 1960. Magnetic anisotropy and fabric of some foliated rocks from S.E. Australia. Pure and Applied Geophysics 47, 30–40.
Taboada, A., Rivera, L.A., Fuenzalida, A., Cisternas, A., Philip, H., Bijwaard, H., Olaya, J., Rivera, C., 2000. Geodynamics of the Northern Andes: subductions and intracontinental deformation (Colombia). Tectonics 19, 787–813.
Tagami, T., 2005. Zircon fission-track thermochronology and applications to fault studies. Reviews in Mineralogy and Geochemistry 58, 95–122.
Tarling, D.H., Hrouda, F., 1993. The Magnetic Anisotropy of Rocks. Chapman & Hall, Great Britain.
Toro, G., Restrepo, J.J., Poupeau, G., Saenz, E., Azdimousa, A., 1999. Datación por trazas de fisión de circones rosados asociados a la secuencia volcano–sedimentaria de Irra (Caldas). Boletín de Ciencias de la Tierra 13, 28–34.
Van der Hammen, T., 1958. Estratigrafía del Terciario y Maeschtrichiano y Tectonogenesis de los Andes Colombianos. Boletín Geológico Ingeominas 6 (1—13), 67–128.
Vermeesch, P., 2004. How many grains are needed for a provenance study? Earth and Planetary Science Letters 224 (3), 441–451.
Villamil, T., 1999. Campanian–Miocene tectonostratigraphy, depocenter evolution and basin development of Colombia and western Venezuela. Palaeogeography, Palaeoclimatology, Palaeoecology 153, 239–275.
Villagómez, D., Spikings, R., Mora, A., Guzmán, G., Ojeda, G., Cortés, E., Van der Lelij, R., 2011. Vertical tectonics at a continental crust-oceanic plateau plate boundary zone: fission track thermochronology of the Sierra Nevada de Santa Marta, Colombia. Tectonics 30 (4) (TC4004, 18 pp.).
Villagómez, D., Spikings, R., 2013. Thermochronology and tectonics of the Central and Western Cordilleras of Colombia: Early Cretaceous–Tertiary evolution of the Northern Andes. Lithos 168, 228–249.
Vinasco, C., Cordani, U., 2012. Episodios de reactivación del sistema de fallas del Romeral en la parte Nor-Occidental de los Andes Centrales de Colombia a través de resultados ^{39}Ar-^{40}Ar y K-Ar. Boletín de Ciencias de la Tierra 32, 111–124.
Wagner, G., Van den Haute, P., 1992. Fission-Track Dating. Dordrecht, Netherlands.
Wegner, W., Wörner, G., Harmon, M.E., Jicha, B.R., 2011. Magmatic history and evolution of the central American land bridge in Panama since the Cretaceous times. Geological Society of America Bulletin 123 (3–4):703–724. http://dx.doi.org/10.1130/B30109.1.
Winkler, A., Florindo, F., Sagnotti, L., 1996. Inverse to normal fabric transition in an upper Miocene marly sequence from Tuscany, Italy. Geophysical Research Letters 23, 909–912.